# Impiego di modelli fisici per lo studio della vegetazione dallo spazio

## Nuove generazioni di sensori e prospettive operative

Francesco Vuolo

TESI DI DOTTORATO

in

***VALORIZZAZIONE E GESTIONE DELLE RISORSE AGRO-FORESTALI***

***Analisi e Modellistica dei Sistemi Agrari e Forestali***

Tutore
Prof. Guido D'Urso
_____

Co-Tutore
Ing. Luigi Dini
_____

Coordinatore del dottorato
Prof. Antonio Cioffi
_____

Francesco Vuolo
_____

**XIX CICLO**
**Università degli studi di Napoli "Federico II"**
**Facoltà di Agraria, Novembre 2006**

# Physically based approaches for monitoring vegetation from space
New generation sensors and operational perspectives

Francesco Vuolo

A thesis submitted to the University of Naples "Federico II"
in partial fulfillment of the requirements
for the degree of

**Doctor of Philosophy**

in

***VALORIZZAZIONE E GESTIONE DELLE RISORSE AGRO-FORESTALI***

***Analisi e Modellistica dei Sistemi Agrari e Forestali***

Tutor
Prof. Guido D'Urso
_____

Co-Tutor
Ing. Luigi Dini
_____

Coordinator
Prof. Antonio Cioffi
_____

Francesco Vuolo
_____

**XIX CICLO**
**University of Naples "Federico II"**
**Faculty of Agriculture, November 2006**

**ABSTRACT**

# Physically based approaches for monitoring vegetation from Space

## New generation sensors and operational perspectives

by
Francesco Vuolo
University of Naples "FEDERICO II", 2006

Professor: Guido D'Urso
Department: Agricultural Engineering and Agronomy

*The use of Earth Observation (E.O.) data to retrieve biophysical variables of land surface such as the Leaf Area Index (LAI) has been proven to be useful in many operative tools to repetitively gather information at spatial and temporal resolution suitable for agricultural applications.*

*In the last years, the diverse capabilities of airborne and satellite remote sensing imagery have been extensively exploited and several approaches have been proposed to estimate the LAI with different accuracy at scales ranging from individual plots to large areas. So far, empirical approaches based on vegetation indices (VI) and alternative approaches based on inversion of physically based radiative transfer models of vegetation have been successfully applied using both airborne and satellite data.*

*The main objective of the work is to exploit the rich information content of CHRIS/PROBA data, both in the directional and spectral domains, to estimate Leaf Area Index. For this purpose, inversion of a radiative transfer model was performed and results compared, in terms of accuracy and operational practicability, to a more empirical approach.*

*Results show that the directional information content improves LAI estimation for two out of three of the analyzed crops. For the best case (corn), it was achieved a LAI RMSE of 0.41 by using 5 angles and 62 spectral bands with an improvement of almost 65% respect to 1 angle and 16 bands. Finally, the accuracy of the LAI estimation for the two approaches was demonstrated to be comparable.*

## Acknowledgments

I gratefully acknowledge everyone who made this research work possible. A very special word of gratitude to Prof. Guido D'Urso for his support and optimism and to Luigi Dini, colleague and friend, for his guidance and long discussions that permitted continuous steps forward.

Thanks also go to the members of the Department of Agricultural Engineering and Agronomy of the University of Naples. I am very grateful to Rosaria Giorgio Gaggia, who taught me the base of image analysis and to Ugo Lazzaro, who supported me in the field measurements work.
Thanks to ESA SPARC campaigns group, especially to the team of the University of Valencia for their contribution in the data correction and planning of the field campaigns.

Finally I wish to thank my parents, Piero and Pina and my all family, Katja and future kinds, who still have to wait to come to life due to the long nights dedicated to science.

## TABLE OF CONTENTS

## LIST OF FIGURES

## LIST OF TABLES

# *Chapter 1*

## 1 Introduction

Biosphere is one of the main components of the Earth's system since it regulates exchanges of energy and mass fluxes at the soil, vegetation and atmosphere level. Global Circulation Models (GCMs), carbon cycle models and water models are exploited to describe, to monitor and to predict environmental factors. These models all use, as input, vegetation biophysical and biochemical parameters for describing $H_2O$ and $C0_2$ fluxes (Hunt et al., 1996; Sellers et al., 1996). These parameters are directly related to plant morphological properties such as leaf area index (LAI), leaf angle distribution (LAD) and vegetation roughness (Sellers, 1989).

The same parameters play also a critical role on a much smaller scale, as in precision farming and water management, to describe the state of plants development and water needs.

The increase of water scarcity - especially for agriculture that accounts for more than 70 per cent of freshwater consumption tapped from lakes, rivers and underground sources - requires a sustainable management of this limited resource.

Therefore, the systematic monitoring of vegetation parameters - that regulate such fluxes - is vital to view water allocation and distribution among users and to make strategic decisions.

Water managers and irrigation engineers need to have accurate and precise estimates of evapotranspiration (ET) to take decisions on water allocation and to design irrigation infrastructures.

The currently most used approach for estimating ET is the so called 'Kc ETo' methodology suggested by the Food and Agriculture Organization (FAO) (Jensen, 1990; FAO, 1998). In order to apply this methodology operatively it is necessary to have accurate measurements of weather parameters (wind speed, air temperature, humidity, solar radiation) as well as precise estimates of vegetation characteristics such as canopy surface albedo, crop height and LAI.

Earth Observation (E.O.) data are definitely a cost-effective source of information to retrieve vegetation parameters required for Kc calculation over in a suitable spatial and temporal resolution (Jochum et al., 2006; D'Urso et al., 2006; Vuolo et al., 2006).

What makes E.O. from satellites so valuable in this context is a high capability of proving systematic observations of the surface. In the last decades, the use of space-technology-based services has filtered through into everyday life with various applications. However, continued

efforts are required, especially for moving from experimental satellites to operational space missions and, by promoting Earth observation market in Europe, to maximize the use of the growing data flow coming from space. Thanks to innovative experimental satellites, processing and modelling techniques, this work wants to demonstrate – focusing on the retrieval of LAI - elements of future monitoring systems and to assess the strengths and limitations of current space missions from a practical and operative point of view.

## 1.1 Overview of the problem

The possibility to quantitatively estimate vegetation parameters by means of optical E.O. data has been explored theoretically by many authors (Sellers, 1985, 1987; Tucker and Sellers, 1986; Choudhury, 1987) and has been followed by numerous other works dealing with the subject.

This work will focus on the retrieval of LAI, which is one of the main variables used to model many processes, such as canopy photosynthesis and evapotranspiration. LAI determines the size of the plant–atmosphere interface and thus plays a key role in the exchange of energy and mass between the canopy and the atmosphere (Monteith and Unsworth, 1990).

LAI is a quantitative measure of the amount of live green leaf material present in the canopy. It is defined as half the total green leaf area (one-sided area for broad leaves) per unit ground surface (Chen and Black, 1992).

Starting from the spectral and directional properties of the vegetation, the following paragraph will give a brief overview of the present status and the applicability of satellite remote sensing for estimating LAI.

## 1.2 Spectral and directional properties of vegetation

The reflectance of plant canopies in the 0.4–2.5 μm wavelength region provides the basis for passive remote sensing of vegetated areas and can be measured from remote instruments such as airborne or spaceborne sensors (Tucker and Sellers, 1986).

In the photosynthesis process green vegetation uses light energy to produce carbohydrates from $CO_2$ and water and releases $O_2$. Photosynthetically active radiation (PAR) (in the 0.4–0.7 μm wavelength range) is able to penetrate in the upper epidermal surface of leaves (Gates et al, 1965; Knipling, 1970; Woolley, 1971; Gausman, 1974), and is absorbed strongly by the plant pigments (chlorophyll a +b, carotenoids).

Thus, absorption is high in the 0.4–0.7 μm region, whereas reflectance and transmittance is low. In the near-infrared part of the spectrum (0.7–1.3 μm), scattering by the structures within the leaves

causes a high reflectance and transmittance since little absorption occurs (Tucker and Sellers, 1986). While liquid water is transparent to the PAR wavelengths, it is a strong absorber in the 1.3–2.5 μm region (Curcio and Petty, 1951). Therefore the water content in the leaf tissues causes absorption in this spectral region.

Tucker (Tucker, 1978) proposed five primary and two transition waveband regions between 0.4–2.5 μm where differences in leaf optical properties (scattering and absorption) and the background optical properties control canopy spectral reflectance. The waveband regions are: (1) 0.4–0.5 μm, where strong spectral absorption by the chlorophyll and the carotenoids occurs; (2) 0.5–0.62 μm, where reduced levels of chlorophyll absorption occur (i.e. why green vegetation to our eyes appears "green"); (3) 0.62–0.7 μm, where strong chlorophyll absorption occurs; (4) 0.70–0.74 μm, where strong absorption ceases; (5) 0.74–1.1 μm, where minimal absorption occurs and the leaf scattering mechanisms result in high levels of spectral reflectance; (6) 1.1–1.3 μm, where the liquid-water coefficients of absorption increase from close to 0 at 1.1 μm to values of 4 at 1.3 μm; and (7) 1.3–2.5 μm, where absorption by liquid water occurs.

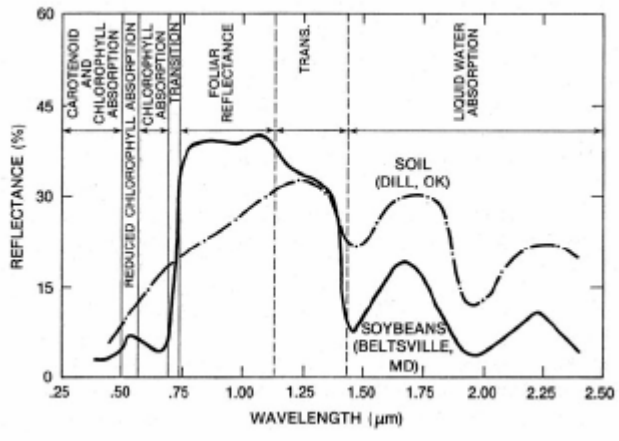


**Figure 1 Typical spectrum reflectance of vegetation**

However, the reflectance of vegetation canopies is not only dependent on plant pigments, the leaf density and the liquid water present (Tucker and Sellers, 1986), but also on the position of the sun (illumination source) with respect to the target and the observer (remote sensors) according to Bidirectional Reflectance Distribution Functions (BRDFs) (Nicodemus et al., 1977). These are equations which mathematically describe how reflectance of a surface varies with the sun-target-sensor geometry.

At leaf level it depends on epidermis characteristics and on the internal structure of the leaves (review in Jacquemoud, 1990). At canopy level the directional reflectance is mainly influenced by

the LAD and the leaf spatial distribution (Chen, 1996). LAD determines the variation of canopy gap fraction with zenith angle. The leaf spatial distribution controls the amount of radiation transmitted through the canopy considering the same LAI.

Multi-directional observations can be the complement to hyper-spectral data to describe the canopy reflectance behaviours and extract useful information.

Recent advances in developments of remote sensing platforms, sensor capabilities (e.g., MISR, POLDER, CHRIS/PROBA) and BRDF modelling (Chopping 2000a; Chopping 2000b; Lucht et al., 2000; Duchemin, 1999; Verstraete et al., 1990) indicate that (not only the hyper-spectral information but also) the directional information can be measured and interpreted. This technical progress may provide improved accuracies relative to single-angle parameter estimation approaches, capitalizing on both the spectral domain as well as the radiometric variations in signal with direction.

In the next paragraph a short overview of vegetation parameters estimation (in particular LAI) from single and multi directional data is given. A discussion of advantages and disadvantages of both approaches is included.

### 1.3 Vegetation indices and canopy reflectance models

Considering the information content of E.O. data, two main approaches have been used to estimate LAI from reflective optical measurements (Verstraete et al., 1996): (1) based on empirical–statistical relationships between LAI and vegetation indices (VI) and (2) on the inversion of radiative transfer models.

Most VI combine information in only two spectral broad bands: in the red (R) and near-infrared (NIR) wavelength region. VIs are established to minimise the effect of external factors on spectral data and have been used to derive canopy parameters such as LAI and fraction of absorbed photosynthetic active radiation (FPAR) (Baret and Guyot, 1991). The most commonly used indices to derive LAI from E.O. data are the Simple Ratio (SR) (Jordan, 1969) and the Normalised Difference Vegetation Index (NDVI) (Rouse et al, 1974). These indices have been found to be well correlated with various vegetation variables including green leaf area (Holben et al, 1980; Asrar et al, 1984, 1985b; Hatfield et al, 1985; Clevers, 1989) and crop coefficient (Calera et.al , 2006). However, they are sensitive to optical properties of soil background (Elvidge and Lyon, 1985; Huete et al, 1985). Therefore several other indices have been proposed to minimise the

effects of soil background, e.g. the perpendicular vegetation index (PVI) (Richardson and Wiegand, 1977), the weighted difference vegetation index (WDVI) (Clevers, 1986, 1989), the soil adjusted vegetation index (SAVI) (Huete, 1988) and the transformed soil adjusted vegetation index (TSAVI) (Baret et al, 1989).

Despite the large effort in improving the performance of such empirical formula, they still present limitations since they are site and sensor specific, require a reliable ground reference data-set to be calibrated and quickly saturate becoming insensitive to variations of LAI at high LAI-values. (Curran, 1994; Gobron et al., 1997). Moreover, VIs can not take into account that the canopy reflectance depends on the canopy structure (LAD, the leaf spatial distribution, row orientation, and spacing), leaf and soil optical properties, sun-target-sensor geometry (Huete, 1987; Bacour et al., 2002).

Furthermore, they are generally based on a few spectral bands and single-angle observation, with a consistent under-exploitation of the full spectral and directional range available in new generation sensors.

Therefore satellite derived indices must be based at least on data corrected or normalized to a "standard" (e.g., nadir) direction and by using site and sensor-specific calibrated relationships.

It can be concluded that the estimation of LAI on the basis of optical remote sensing is not straightforward, although it is the only way to obtain LAI in a large spatial scale.

Alternative approaches based on canopy reflectance models represent a challenging opportunity for the estimation of vegetation parameters from E.O. data with high dimensionality (both in the spectral and the directional domains).

A canopy reflectance (CR) model describes the transfer and interaction of electromagnetic radiation inside the canopy based on physical laws. Some reviews, presented in next paragraph, were made by Goel (1988), Myneni (1989) and recently by Lewis.

A CR model can be used in the direct mode and in the inverse mode. In direct mode, the canopy reflectance is simulated based on a specific set of (biophysical) input parameters. In inverse mode, observed canopy reflectance is used to retrieve these biophysical parameters.

On the one hand, the physical approach permits a higher validity since there is no restriction by empirical relationship. Additionally, it offers the potential to exploit directional information by analyzing the distinctive features of the surface BRDF.

On the other hand, there are also several limitations. The parameter retrieval performance requires sufficient sampling of the surface BRDF, with the associated requirement for good calibration and atmospheric correction. It depends both on the CR model accuracy and the inversion algorithms (Kimes es al., 2000), which have to be both fast and robust enough to avoid problems in the minimization of the error function.

A short overview of CR models is given in next paragraph followed by most common issues on non-linear model inversion.

## 1.4 Overview of canopy reflectance models

Due to the importance of CR modelling for this study, an overview about various models developed in the last years will be given in this section.

Since the first CR model was formulated by Monsi and Saeki (1954), a large number of physically based canopy reflectance models with increasing levels of complexity have been developed. Recent reviews have been given by Casa (2003) and Lewis (1996), following Goel (1988), Myneni et al. (1989), Myneni and Ross (1991).

Generally, models of canopy reflectance can be categorized into five major types, whereas some include features from the others:

**(1) Empirical Models:**

Starting from the simplest approach, this kind of models are based on empirical functions which only assume the form of realistic reflectance distributions (see Walthall et al., 1985; Roujean et al., 1992 and Rahman et al., 1994). Thus, the mathematics is not physically-based even though "layers" of functions can be added to specifically account for the scattering phenomena (e.g., the ‘hot spot’). Inversion of empirical models have been carried out to estimate surface albedo and/or to correct for surface anisotropy.

**(2) Turbid Medium Models:**

Increasing the complexity, turbid medium models might be regarded as a first step of a physically based description of canopy reflectance. These models describe a series of plane parallel horizontal layers composed of small randomly distributed infinitesimal elements, with defined

optical properties (absorbing and scattering), oriented in given directions (Goel 1989). Their angular distribution can be defined according to the LAD of true canopies (Ross and Nilson 1966).

Turbid medium models are generally able to describe single and multiple scattering. While the first can be determined quasi analytically, the second is based on approximations.

A disadvantage of the turbid medium approach is the absence of scattering behaviour caused by the finite size of actual scatterers (e.g., shading) and the non-random orientation of scatterers (e.g., leaf clumping). In consequence, the models are more suitable to simulate reflectance characteristics of continuous uniform vegetated covers, such as crops or dense canopies, than to describe heterogeneous vegetation structures.

A benefit of these models is their mathematical simplicity and thus computational efficiency. Thus, inversion of these models has been carried out by many authors.

**(3) Geometric-Optical Models:**

These kinds of models are based on a ground surface with known reflective properties. The canopy above this surface is described by geometrical objects of different shapes (such as cylinders, spheres, cones, cubes, ellipsoids, etc.). (see e.g., Otterman, 1984; Li and Strahler 1985; 1992; Jasinski, 1990).They further consider that illuminated and shadowed proportions of a scene vary depending on view and illumination angles, determining the directional reflectance. The optical properties (transmittance, reflectance and absorption) are described a in a defined manner.

Reflectance anisotropy is determined primarily by the fractions and spatial orientation of shaded and sunlit surfaces (both canopy and ground) for a particular sun-target-sensor geometry. They are most suitable for sparse canopies or clods of soil. The geometric-optic approach was original developed as alternative for radiative transfer models, taking into account more complex vegetated land surfaces (Li and Strahler, 1995).

Geometrical models have been inverted to retrieve canopy structure parameters (Li and Strahler, 1985; Wu and Strahler, 1994; Hall et al., 1994) and optical information (Otterman et al., 1987).

**(4) Hybrid Models:**

Hybrid models combine the spatial heterogeneity of geometrical models with the realistic transport treatment of turbid medium models. This permits the simulation of gap probabilities and path length distributions along with single and multiple scattering (e.g., Norman and Welles, 1983; Li

et al., 1994). Nevertheless, this complexity results in relatively high computational expense. Thus, operational inversions of these models appear impractical.

**(5) Computer Simulation Models:**

This approach depicts the highest level in complexity in describing canopy reflectance characteristics and the heterogeneous BRDF problem. By means of computer simulation models the arrangement and orientation of canopy elements is based on a three dimensional description. They rigorously trace photon interactions with an arrangement of discrete scatterers.

Although computationally intensive, these models accurately simulate within-canopy spatial heterogeneity (e.g., organ size distributions, leaf clumping, gaps) and scene-scale heterogeneity (e.g., topography) that other models must either neglect or approximate with quasi-empirical formulations. Several models have been developed (see Ross and Marshak, 1988; Goel et al., 1991; Borel et al., 1991; Lewis and Muller, 1992), but their high computational demand hamper the applicability for inversion purposes (Antyufeev and Marshak, 1990).

Concluding, numerous modelling approaches have been worked out to describe the interaction of radiation with canopies, basing on a range from simple empirical to highly complex methodologies.

Referring to the objective of this work, a complexity higher than the turbid medium approach is presently questionable for operational applicability. For this reason, geometric-optical, hybrid and computer simulation model approaches will not be taken into account in further analyses of the present study. This does not exclude that in the future these kinds of models may play an important role in deriving information from E.O. data.

## 1.5 Canopy reflectance model inversion

By means of model inversion, information on surface parameters can be obtained from observed E.O. data. There are many issues about model inversion. The main concept behind it was given by Goel (1989). According to the Least-Square Error method, a cost function is defined to provide a measure of "goodness of fit" as follows:

$$F = \sum_{i=1}^{n} \omega_i \left[ \rho_{obs\,i} - \rho_{meas\,i} \right]^2 \qquad \textbf{Eq. 1}$$

where $\rho_{obs,i}$ and $\rho_{meas,i}$ are the observed canopy reflectance for n spectral bands and the corresponding modelled canopy reflectance, respectively. $\omega_i$ is the weight given to an observation. Each residual should be weighted by the uncertainty associated with the observation i.

If the model accurately represents canopy reflectance, and there are no measurement errors, the value of the cost function should approach to zero. If the relation between canopy reflectance and the set of input canopy parameters is not unique, (i.e. there are more than one minima), the model is not mathematically invertible.

Often there is no analytical solution to the (multidimensional and non-linear) simultaneous equations obtained from the partial differentiation of CR models. Thus, the inversion of CR models is by nature an ill-posed problem. That means different model parameter combinations can produce almost identical spectra (Combal et al., 2002; D'Urso, 2004a). Baret (Baret & Guyot, 1991) for instance, demonstrated that the spectral reflectance of sparse canopy with mostly horizontal leaf orientation is similar to a dense canopy with mostly vertical leaf orientation. The average deviations between model generated spectrum and retrieved spectra resulted very small showing that different sets of parameters can correspond to almost similar spectra.

However, different methodologies have been proposed for the inversion and for the regularization of the ill-posed problem, e.g. based on the constraining to fixed values of some parameters, on the use of a-priori knowledge, taking into account the temporal evolution of the crop cycle. Another possibility is the object-based retrieval of canopy parameters, considering the radiometric information of neighbouring pixels during model inversion. (review in Kimes es al., 2000; Combal et al., 2002; CROMA, 2000; Atzberger, 2002, 2004).

Regardless of the choice of minimisation method, there are a number of general issues that must be considered when inverting canopy reflectance models (reviews in Lewis et al. 2003).

To find out the minimum of the cost function, there are different kinds of optimization routines that can be exploited, e.g. Quasi-Newton methods, Genetic Algorithms (GAs), Look-up Table (LUT) and Artificial Neural Networks (ANNs).

Quasi-Newton methods start to search space around a single starting point and explores all the local information, in particular the gradient to find the better next point. GA use population of candidate solutions initially distributed over the whole function and identify the sub-domain in which the global minimum can be located. The optimisation problems are expressed as non-linear 'fitness for survival' functions, and genetic mutation and propagation applied to find the 'fittest' parameter values as can be in nature. LUT method consists in generating a discrete set of possible canopy reflectance combinations and storing corresponding parameter values in a table. Optimisation is then based on the comparison of the values in the table with measured data. (Knyazikhin et al, 1998; Pragnere et al, 1999). ANN are non-physical methods that relate a set of input variables to a set of output variables by a learning process. (Abuelgasim et al., 1998; Smith, 1993). They present a training data consisting of canopy reflectance value inputs and true parameter outputs.

Selecting the right inversion algorithm and strategy for a particular problem is of crucial importance in parameter estimation.

## 1.6 Objective of the work

Due to the mechanisms outlined above, inversion of canopy reflectance models is an ill-posed problem and it needs to be regularized to get reliable results.

Simultaneous directional observations, containing information both on the geometrical and structural characteristics of the surface, can better characterize the anisotropic reflectance behaviours over vegetation canopies. Therefore they may contribute, for instance, to uncouple one of the counterbalancing effects between LAI and LAD on reflectance signal. In this sense, multi-directional information should smooth the ill-posed inverse problem.

An agile satellite (PROBA) and a highly configurable sensor (CHRIS) offers the unique potential to acquire high spatial resolution, spectral BRDF data sets and, from these, to study the biophysical and biochemical properties of vegetation canopies. It also provides an important means of validating similar data sets from other, coarser spatial resolution sensors, such as VEGETATION, POLDER2, MODIS and MISR.

Thus, in exploiting the unique and innovative hyper-spectral and multi-angular information content of CHRIS/PROBA imagery, the aim of this research is to estimate LAI by inverting a

canopy reflectance model and to compare the results, in terms of accuracy and operational practicability, to a more empirical approach based on VI.

# *Chapter 2*

## 2 Materials and Methods

### 2.1 Experimental campaign: the SPARC experience

#### *2.1.1 Overall description of the area*

The ESA Spectra Barrax Campaigns (SPARC) [Moreno et al., 2004] were carried out in Barrax (N30°3', W2°6'), an agriculture test area situated within La Mancha region in the South of Spain, from 12 to 14 July 2003 and from 14 to 16 July 2004.

Agricultural research has been concentrated in this area for many years thanks to its flat topography (differences in elevation range up to 2 m only) and to the presence of large and uniform vegetation fields (e.g., alfalfa, corn, potato, sugar beet, onion and garlic) with a wide range of LAI from 0.5 up to 6.5. The area consists of approximately 65% rain fed and 35% irrigated land with different agricultural fruits. The regional water table is located approximately 20-30 m below the land surface. The typical climatic conditions of the Mediterranean area can be found: high precipitations in spring and autumn with a summer minimum. The annual average rainfall is about 400 mm.

#### *2.1.2 Ground data measurements*

During SPARC campaign a large amount of ground measurements were collected in the Barrax study area covering leaf water content, leaf biomass, leaf $Chl_{a+b}$, LAI and fCover (Fernández et al., 2005).

Leaf water content and dry matter measurements were carried out on 3 samples per Elementary Sampling Unit (ESU) collected from a pre-defined area and stored into plastic bags. Each sample was weighted within a few hours and digital photographs of the leaves over squared paper were taken for the calculation of the leaf area. Samples were dried at 70ºC, until constant weight was reached, and then weighted again. From the two masses and the known sampled area, water and dry matter content were calculated.

The leaf chlorophyll content was measured with the CCM-200 Chlorophyll Content Meter. It performs relative measurements, so that a calibration should be made by using laboratory analysis methods (Gandia et al., 2005).

Field non-destructive measurements of LAI and Mean Tilt Angle (MTA) were made by means of the digital analyzer LI-COR LAI-2000 (LI-COR Inc., 1992); the manufacturer's recommendations were followed in deciding sampling strategy. In order to reduce the effect of multiple scattering on LAI-2000 measurements, the instrument was only operated near dusk and dawn (6:30-9:30 am; 6:30-8:30 pm) and under diffuse radiation conditions using one sensor for both above and below canopy measurements. In order to prevent interference caused by the operator's presence and the illumination condition, the sensor field of view was limited with a 180° view-cap. Both measurements were azimuthally oriented opposite to the sun azimuth angle. Twenty four samples of LAI measurements were taken, comprising one full set of measurements in each ESU. Each centre of the LAI-2000 transects was geolocated by using GPS measurements as showed in .
A summary of the biophysical parameters measured for the characterization of the different crops during SPARC-2003 is shown in Table 1. The strategy sampling is described in detail in SPARC campaign handbook.

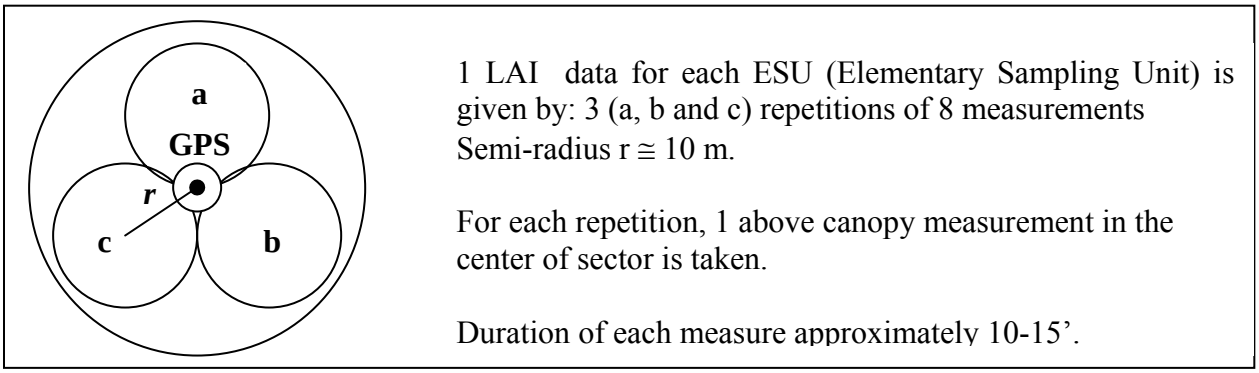


**Figure 2 Leaf Area Index protocol measurements**

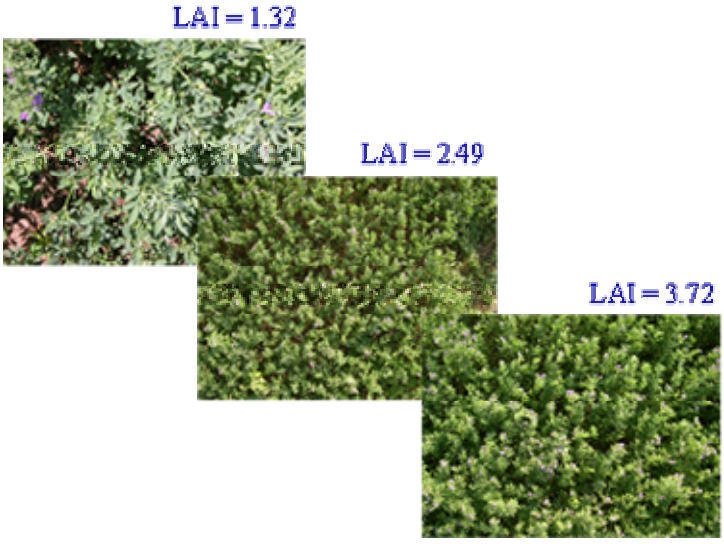


**Figure 3 Examples of LAI values for alfalfa canopies**

| Crop | ESU | Chlorophyll Mean Value (µg cm$^{-2}$) | Crop Mean Values (µg cm$^{-2}$) |
|---|---|---|---|
| Corn | C1-A1 | 48.9 ± 0.5 | 50.6± 0.8 |
| | C1-A2 | 51.6 ± 0.5 | |
| | C1-A3 | 50.4 ± 0.4 | |
| Sugar - beet | B1-T1 | 44.9 ± 1.0 | 44.3 ± 1.4 |
| | B1-T2 | 48.6 ± 0.9 | |
| | B1-T3 | 42.5 ± 1.2 | |
| | B1-T4 | 43.4 ± 1.0 | |
| | B1-T5 | 38.8 ± 1.0 | |
| | B1-T6 | 47.4 ± 0.8 | |
| Onion | On1-B1 | 23 ± 3 | 20 ± 2 |
| | On1-A1 | 23 ± 4 | |
| | On1-B2 | 20 ± 3 | |
| | On1-B4 | 16 ± 3 | |
| | On1-B5 | 18 ± 3 | |
| | On2-A1 | 22 ± 3 | |
| | On2-A2 | 6 ± 2 | |
| Garlic | G1-A7 | 20 ± 2 | 15 ± 2 |
| | G1-A8 | 15.0 ± 1.6 | |
| | G1-A9 | 12.5 ± 1.7 | |
| | G1-A10 | 11.0 ± 1.6 | |
| Potato | P1-T12 | 36.7 ± 0.7 | 35.6 ± 0.5 |
| | P1-T11 | 36.0 ± 0.5 | |
| | P1-T10 | 35.4 ± 0.8 | |
| | P1-T9 | 34.4 ± 0.6 | |
| Alfalfa | A9-T0 | 48.5 ± 1.2 | 48.5 ± 1.2 |

| CROP | DM Range of values (g m$^{-2}$) | DM µ±σ (g m$^{-2}$) |
|---|---|---|
| Corn | 53.9 - 69.9 | 61 ± 6 |
| Alfalfa | 55.5-106.1 | 89 ± 23 |
| Alfalfa | 47.1 - 90.4 | 65 ± 19 |
| Potato | 39.7- 46.1 | 43 ± 3 |
| Onion | 71.4 - 89.4 | 83 ± 7 |
| Sugar beet | 50.5 - 86.4 | 72 ± 11 |
| Garlic | 99.8 -189.5 | 130 ± 33 |

| CROP | WC Range of values (g m$^{-2}$) | WC µ±σ (g m$^{-2}$) |
|---|---|---|
| Corn | 165.9-189.5 | 180 ± 18 |
| Alfalfa | 110.9-160.3 | 140 ± 68 |
| Alfalfa | 105.9-142.8 | 126 ± 45 |
| Potato | 213.8-240.4 | 223 ± 21 |
| Onion | 602.9-810.1 | 680 ± 152 |
| Sugar beet | 315.1-635.6 | 400 ± 117 |
| Garlic | 482.1-712.1 | 600 ± 142 |

**Table 1 Biophysical characterization of crops during SPARC-2003**

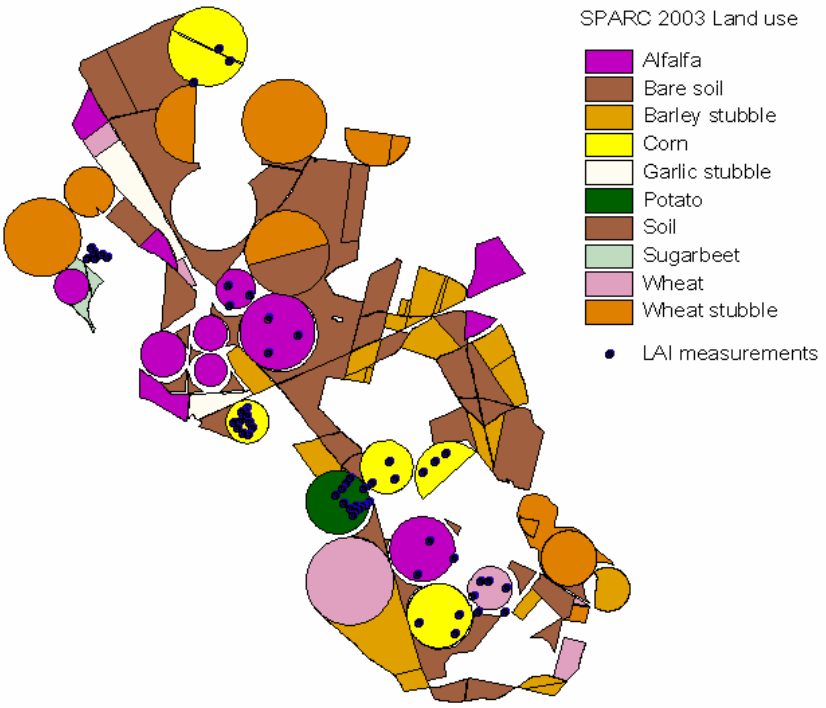


**Figure 4 Land use classification during SPARC-2003 and LAI measurement points**

### *2.1.3 Earth Observation (EO) data: CHRIS/Proba imagery*

The European Space Agency's (ESA) Project for On-Board Autonomy (PROBA) is a technology demonstration experiment to take advantage of autonomous pointing capabilities of a generic platform suitable for Earth observation purposes. Among different sensors, the PROBA instrument payload includes the Compact High Resolution Imaging Spectrometer (CHRIS). The coupled PROBA/CHRIS system, launched on October 22, 2001, provides high spatial resolution hyper-spectral and multi-angular data, that constitutes a new generation of remote sensing information to be processed and exploited.

PROBA platform provides pointing in both across-track and along-track directions. In this way, PROBA/CHRIS system has multi-angular capabilities, acquiring up to five consecutive images from five different view angles in the same satellite overpass. Each imaged target has an associated "fly-by" position, which is associated to that position on the ground track where the platform zenith angle, as seen from the target, is a minimum [i.e., minimum zenith angle (MZA)]. The platform acquires the images at times when the zenith angle of the platform with respect to the fly-by position is equal to a set of fly-by zenith angles (FZA): 0 , ± 36, or ± 55. Negative MZA values correspond to target locations east of the ground track, and negative FZAs to acquisition geometries when the satellite already passed over the target position. A schematic view of PROBA/CHRIS acquisition geometry is displayed in Figure 5.

On the other hand, CHRIS measures over the visible/near-infrared (NIR) bands from 400–1050 nm, with a spectral sampling interval ranging between 1.25 (at 400 nm) and 11 nm (at 1000 nm). It can operate in different modes, reflecting a necessary compromise between spatial resolution and the number of spectral channels, caused by limits to onboard storage.

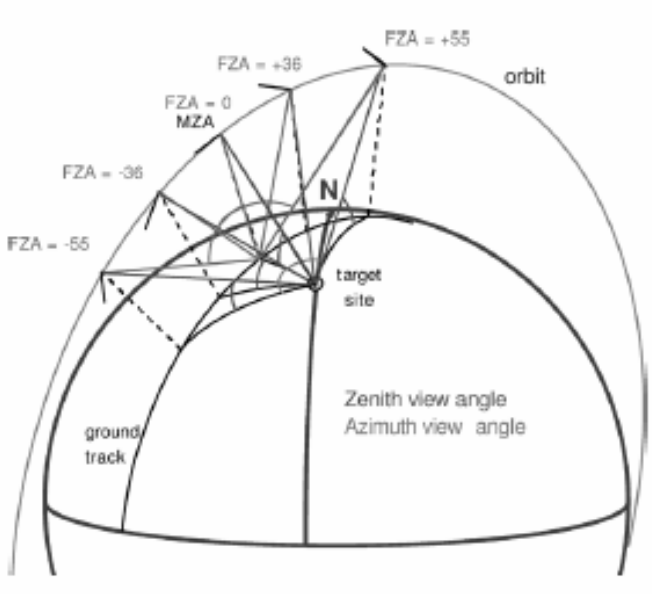


**Figure 5 Scheme of CRHIS/PROBA acquisition geometry (Guanter et al., 2005)**

For this study we worked with a set of five hyper-spectral consecutive CHRIS/PROBA images collected on 14 July 2003 at 11:32 GMT from five different view angles during a single orbital overpass. These images (namely "A1", "A2", "A3", "A4", "A5") were acquired in Mode-1 with a spectral resolution of 62 bands over the visible/near-infrared bands from 400–1050 nm, in a spatial resolution of 34 m. The acquisition geometry for the images is shown in Table 2 and Figure 7.

| | Minimum satellite zenith angle | | | | |
|---|---|---|---|---|---|
| | A1 | A2 | A3 | A4 | A5 |
| 14/07/2003 | 57,3 | 42,4 | 27,6 | 42,5 | 57,4 |

**Table 2 CHRIS/PROBA acquisition geometry**

The image closer to nadir, "A3", was acquired with a view zenith angle equal to 27,6°.

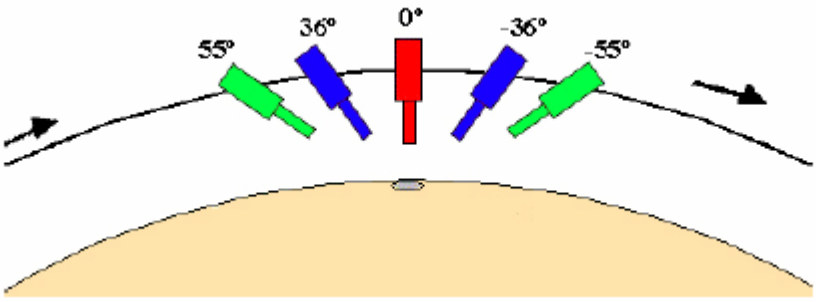


**Figure 6 Simplified schematization of multiangular acquisitions from CHRIS/PROBA.**

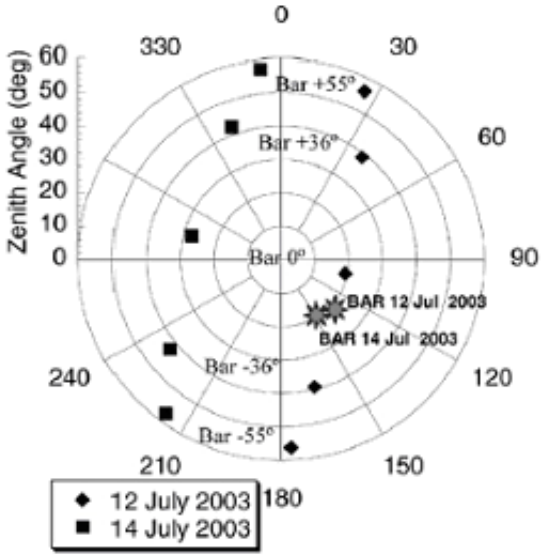


**Figure 7 Directional sampling of CHRIS/PROBA for SPACR-2003 on 14 July 2003 at 11:30 GMT**

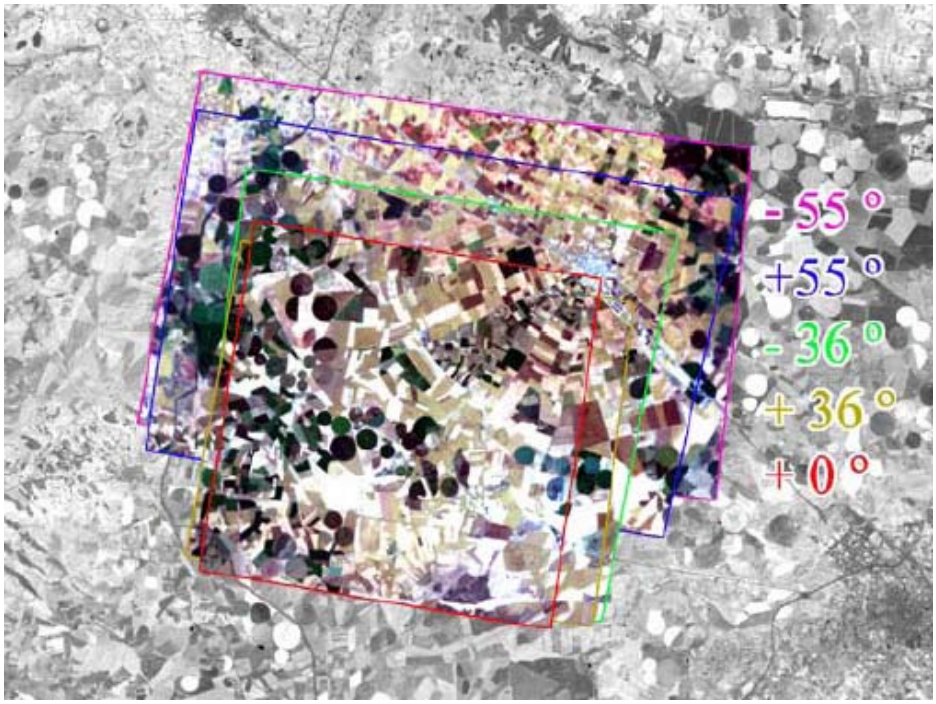


**Figure 8 CHRIS/PROBA imagery acquired on 14th July 2003**

Radiometric calibration, atmospheric and geometric correction of CHRIS imagery was performed by the Department of Thermodynamics of the University of Valencia. Since important calibration problems were reported in several CHRIS channels data, a dedicated atmospheric correction algorithm was applied jointly with radiometric calibration of the data in an autonomous process, without the need for any ancillary data (Guanter et al., 2005).

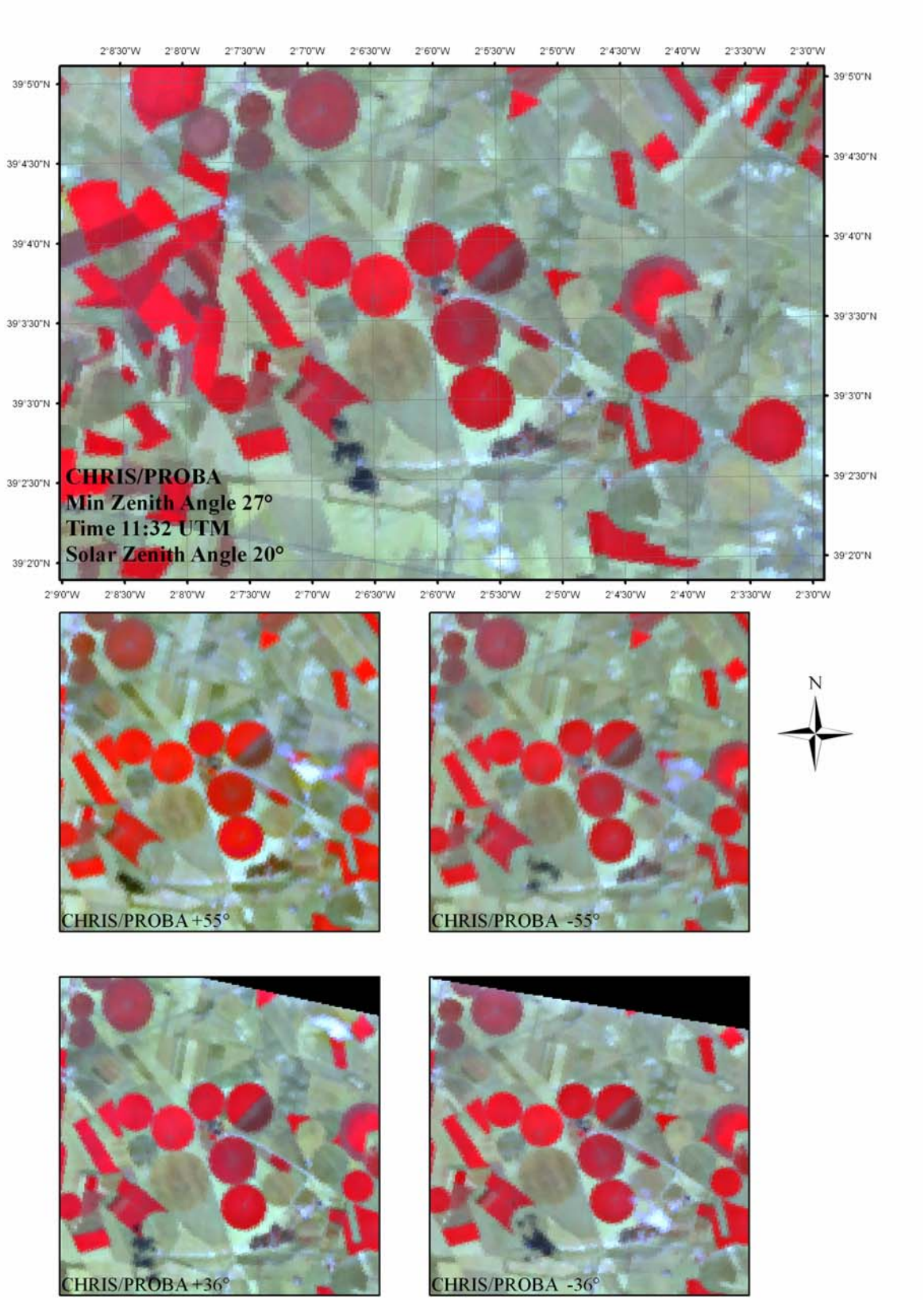


**Figure 9 CHRIS/PROBA imagery over BARRAX – 14 JULY 2003**

*2.1.3.1 Directional sampling of BRDF from CHRIS/PROBA*

To obtain a BRDF feature representative to the true properties of ground object, it is necessary to perform a spatial average to the georeferenced multi angular images. In fact, because of the limitations of registration, pixel alignment and the intrinsic scale of scene, to extract BRDF features from georeferenced image without average is not recommended (Qiang et al., 2003). Thus a set of surface reflectance was extracted from CHRIS images considering an average filter of 3*3 pixels. An example of the BRDF features of different surface in shown in Figure 10 and Figure 11.

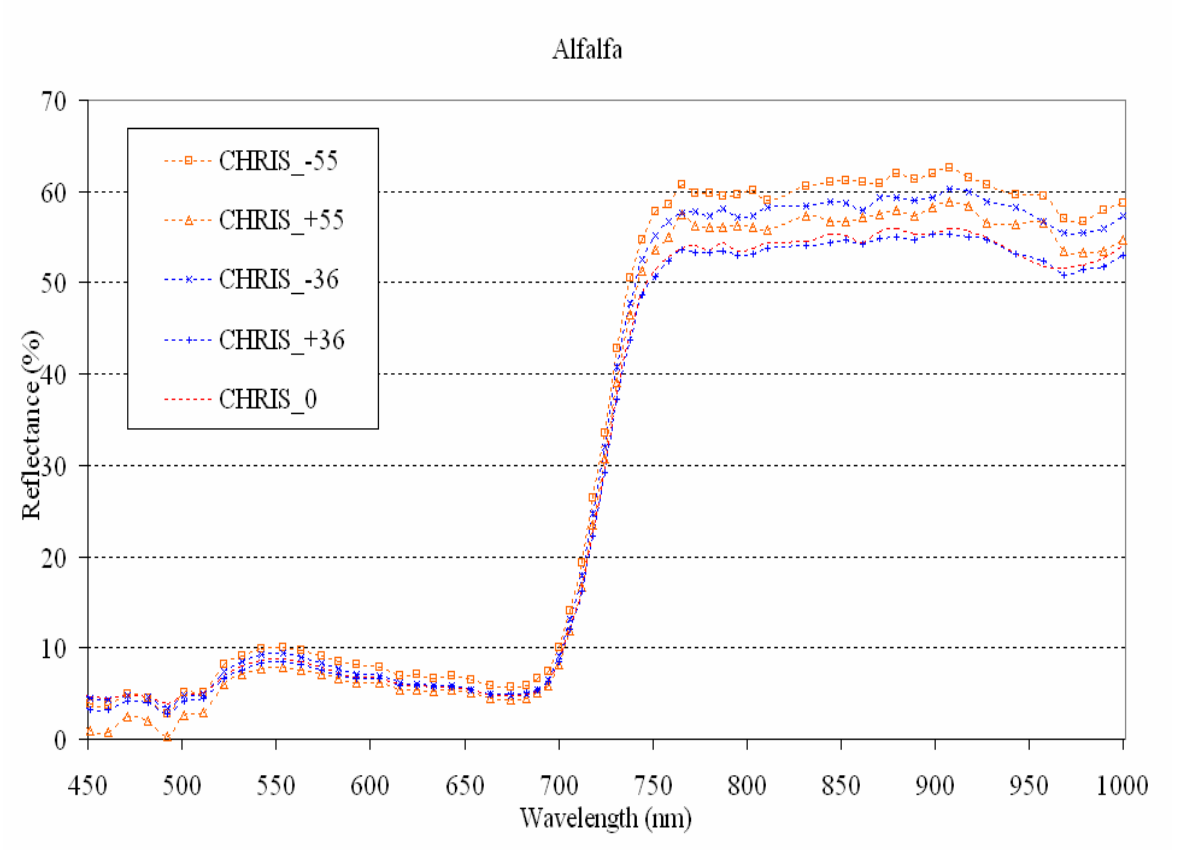


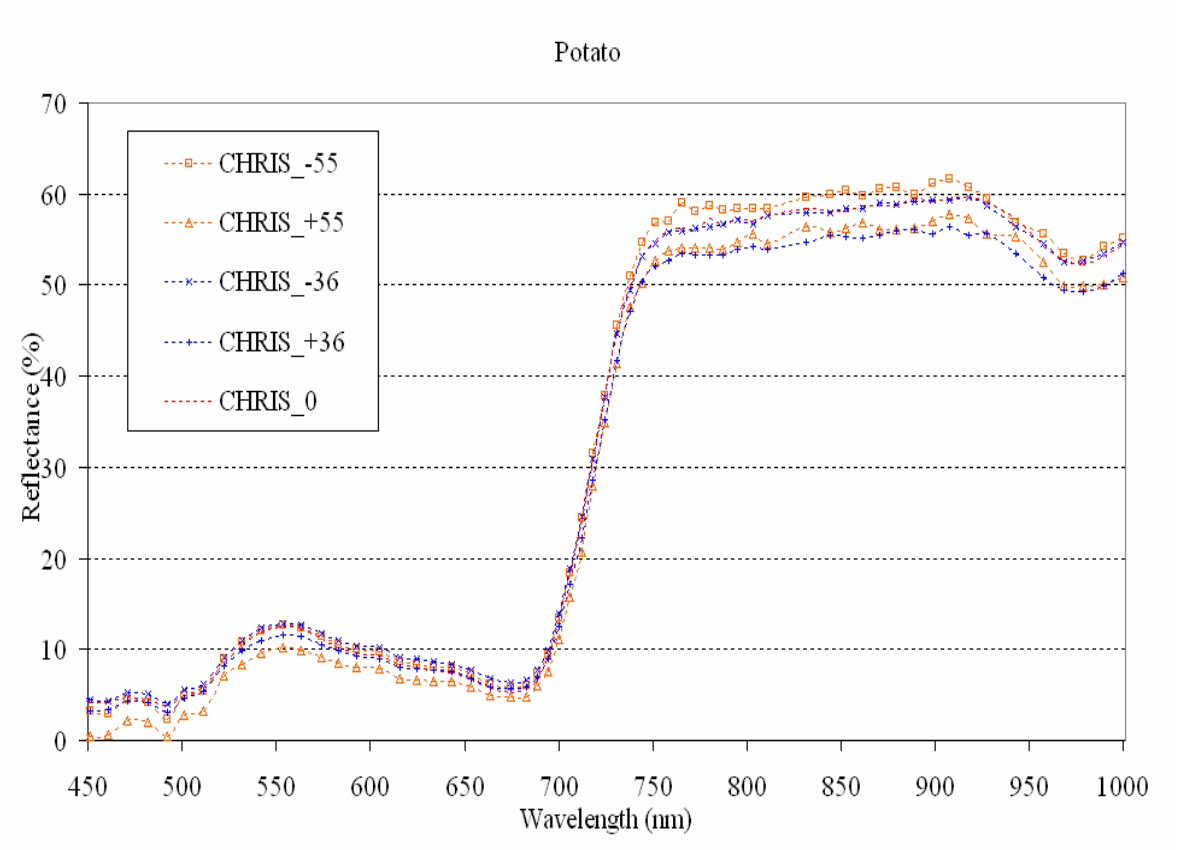


**Figure 10 CHRIS/PROBA spectral and directional reflectance acquired by CHRIS/PROBA over Barrax site on 14 July 2003 at 11.30 GMT.**

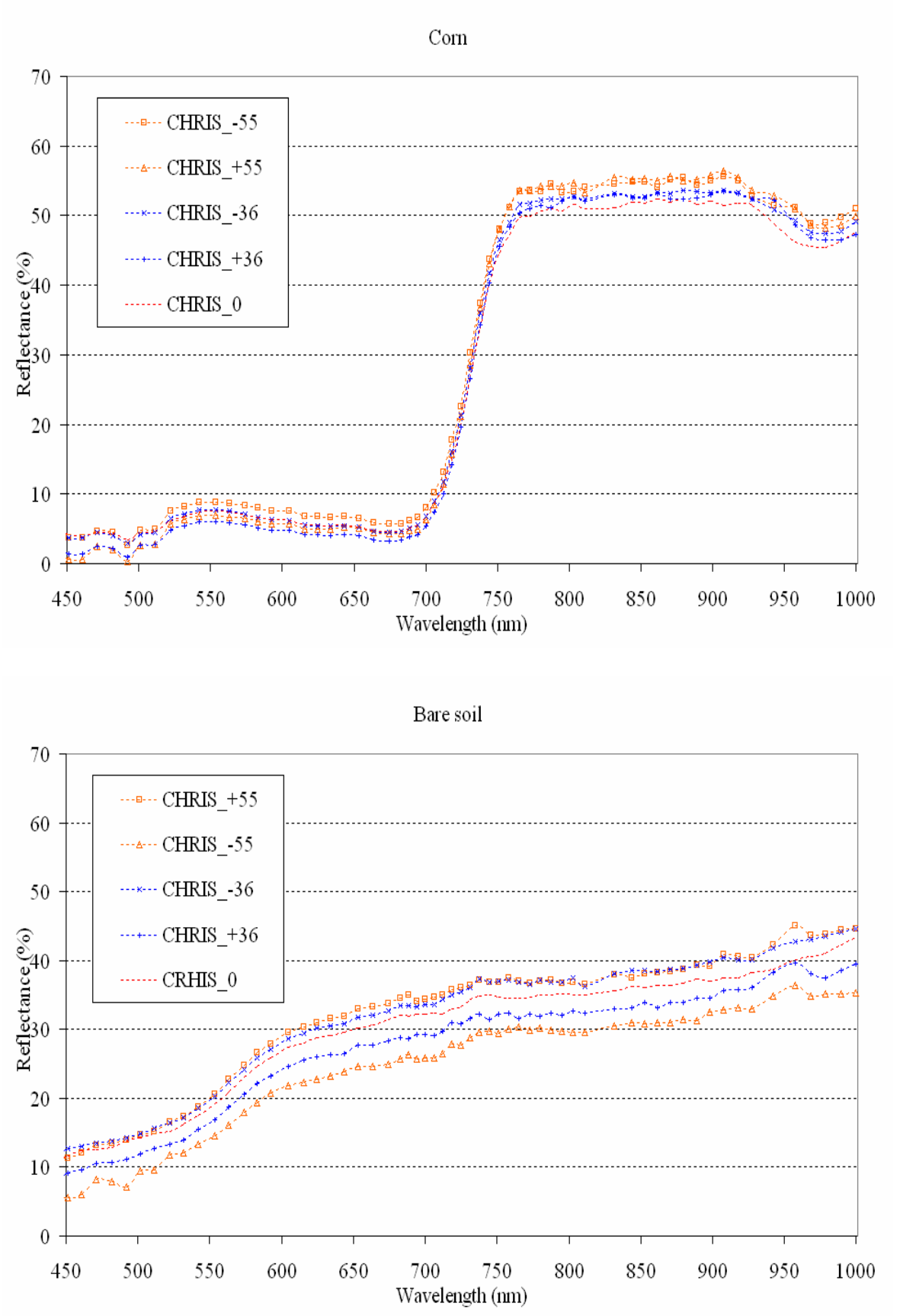


**Figure 11 CHRIS/PROBA spectral and directional reflectance acquired by CHRIS/PROBA over Barrax site on 14 July 2003 at 11.30 GMT.**

## 2.2 Canopy Reflectance Modelling.

For the purpose of this study two well known reflectance models were used: the PROSPECT model (Jacquemoud et al., 1990) for the simulation of the leaf reflectance and transmittance coupled with the one-dimensional canopy reflectance model SAILH (Verhoef, 1984, 1998) adapted to take into account the hotspot effect and the multiple scattering in the canopy (kuusk, 1991) (PSH model).

The SAILH model was selected considering the results of the RAMI experiment (The RAdiation transfer Model Intercomparison) (Pinty et al., 2000), that carried out modelling exercises for both structurally homogeneous and heterogeneous canopies.

Two fundamental criteria were considered to choose the coupled version of the PROSPECT and SAILH models: i) simplicity, i.e. the possibility to have a rather good representation of the radiative transfer of the canopy using a relatively small amount of input parameters as well as limited computational requirements (performing numerous calculations with minimum time), and ii) reliability since the SAILH model has been successfully tested for a large set of crops, among them corn (Major et al., 1992) and sugar beet (Andrieu et al., 1997) which were present in our study-area.

### *2.2.1 SAILH and PROSPECT models*

The SAILH model (Verhoef, 1984, 1998) assumes the canopy as a horizontal, homogenous and infinitely extended vegetation layer (turbid medium), made up of Lambertian scatterers (leaves) randomly distributed within the canopy. The radiative transfer equation is solved by the four-stream approximation method: ascending and descending fluxes of direct and diffuse radiation are considered.

The SAILH model requires few parameters; such as single leaf hemispherical reflectance and transmittance ($\rho$, $\tau$), leaf area index (LAI), average leaf angle (ALA), geometric parameters (the solar zenith, the view zenith angles and the azimuth angle between sun and observer, hotspot parameter (hot), introduced by Kuusk (Kuusk, 1991), the fraction of diffuse radiation ($E_{SKY}$) and soil hemispherical reflectance ($\rho_{soil}$). A reflectance factor ($\alpha_{soil}$) was introduced to scale the mean measured soil spectrum accounting for variances in soil brightness.

The PROSPECT model (Jacquemoud et al., 1990) provides the leaf hemispherical reflectance and transmittance to the SAILH model as a function of the leaf structural parameter ($N$), the leaf chlorophyll a+b concentration ($Chl_{a+b}$), the equivalent water thickness ($C_w$) and the dry matter content ($C_m$).

Figure 12 shows the schematization of the coupled PROSPECT and SAILH models, integrating the required input information

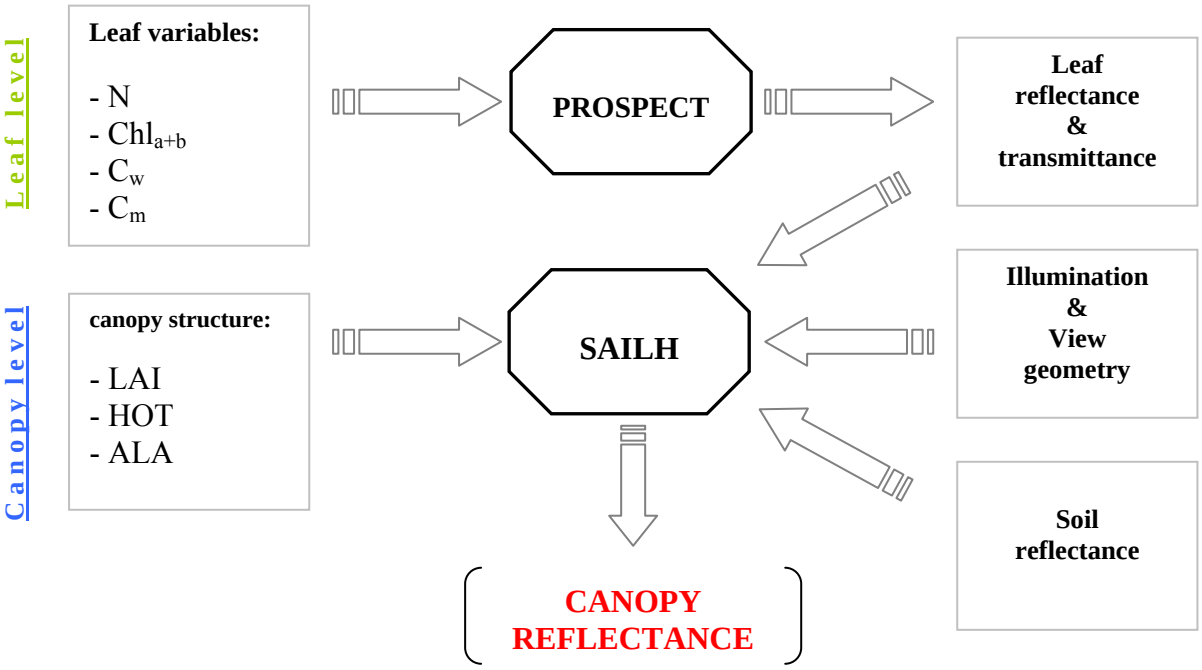


**Figure 12 Schematization of the direct mode of PROSPECT and SAILH models (PSH).**

### *2.2.2 Issues on model inversion*

The ability to determine canopy parameters correctly depends on model accuracy and capability to reproduce the experimental data, appropriate sampling of the surface BRDF and finally it depends on model inversion parameterization.

If the solution is not unique and stable, the model may not be invertible for the given problem configuration (Goel, 1988). The uniqueness and the stability of a solution are determined by the presence of local minima in the model parameter space. These minima represent incorrect parameter combinations for which model spectra resemble the measured data. Solution stability requires that the global minimizer not change significantly for reasonable errors in the data.

CHRIS/PROBA data may provide the potential to overcome some of the difficulties associated with physical-based model inversion from satellite data. First, high spatial resolution of the instrument could facilitate the application of CR models, since there are fewer problems with sub pixel mixtures of land cover type than for “moderate” resolution sensors. Secondly, five views of a

fixed point on the Earth surface can be obtained in a single orbital over-pass. CHRIS/PROBA provides both hyperspectral and directional sampling, which can be expected to have greater information content than each domain alone (Barnsley *et al.* 1997). Furthermore, simultaneous directional observations, which better characterize the anisotropic reflectance behaviour of vegetation, should so contribute to uncouple the counterbalancing effect between LAI and ALA on spectral signal.

In this sense, multidirectional information should smooth the ill-posed problem. Thus, the only regularization taken into account in this study will be a physical coherent bound on the parameter values.

### *2.2.3 Inversion algorithm*

A traditional Levenberg-Marquardt algorithm (LMA) (Levenberg, 1944; Marquardt, 1963) was implemented in order to retrieve LAI by inverting the PSH model.

The LMA interpolates between the Gauss-Newton algorithm (GNA) and the method of gradient descent. The LMA is more *robust* than the GNA, which means that in many cases it finds a solution even if it starts very far off the final minimum. On the other hand, for well-behaved functions and reasonable starting parameters, the LMA tends to be a bit slower than the GNA.

The solution is achieved by iteratively running the PSH model in direct mode and comparing the model output with the acquired CHRIS spectra until an optimal parameter set is found. The optimal parameter set is defined as this combination of canopy variables for which the cost function value is reduced to a minimum. The selected cost function is a simple least square function defined as the sum of squared deviations between model-generated observations and satellite observations:

$$C = \sum_{i=1}^{nb} \sum_{j=1}^{nd} (\rho_{i,j,obs} - \rho_{i,j,\mathrm{mod}})^2 \qquad \textbf{Eq. 2}$$

where $n_b$ is the number of spectral bands, $n_d$ is the numbers of view directions and $\rho_{\mathrm{mod}}$ expresses the modelled reflectance for the sun-sensor geometry corresponding to the observed reflectance $\rho_{\mathrm{obs}}$. The smaller the cost function value the greater is the consistency between model and observations. To start off the inversion process, the algorithms need an initial guess for the parameter vector **x** as well as their lower and upper bounds (summarized in Table 3).

### *2.2.4 Parameterization and setup*

PSH model requires eight parameters and a given geometric configuration. The N and HOT parameter value bounds were left as broad as possible since no field measurements is possible to perform due to their uncertain physical nature. $Chl_{a+b}$ is allowed to vary between 30 and 70, $C_w$ between 0.015 and 0.1 and $C_m$ between 0.001 and 0.01. The $E_{SKY}$ parameter (diffuse part of the incoming radiation) is fixed to 0.16 independent of the wavelength considering local irradiance measurements. The parameters to be retrieved by model inversion, LAI and ALA, are allowed to vary in the range 0.1 – 6.5 and 30° – 80° (starting point 0.1 and 30°), respectively.

The parameter settings take into account field and intra-fields variability from *in situ* measurements and were conservatively expanded. In Table 3 all input parameters with corresponding bounds are listed.

| Parameters | Units | Initial values | Lower bounds | Upper bounds |
|---|---|---|---|---|
| N | - | 1.3 | 1.3 | 2.0 |
| $Chl_{a+b}$ | $\mu g\ cm^{-2}$ | 30.0 | 30.0 | 70.0 |
| $C_w$ | $g\ cm^{-2}$ | 0.015 | 0.015 | 0.100 |
| $C_m$ | $g\ cm^{-2}$ | 0.001 | 0.001 | 0.010 |
| LAI | $m^2\ m^{-2}$ | 0.1 | 0.1 | 6.5 |
| HOT | - | 0.0 | 0.0 | 1.0 |
| ALA | Deg. | 30 | 30 | 80 |
| $\alpha_{soil}$ | - | 0.80 | 0.80 | 1.20 |

**Table 3 Input parameters, units, initial values and bounds.**

The input soil reflectance is calculated averaging spectral samples of soils measured by means of a field spectrometer during the campaign. A wavelength-independent scaling factor, $\alpha_{soil}$, is left free to vary in a range of ±20% from the mean.

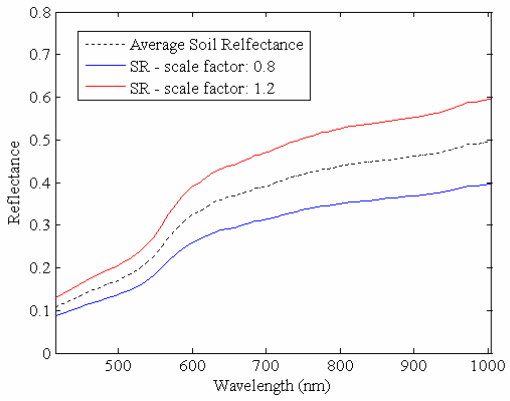


**Figure 13 Average soil reflectance used as input in the inversion of PSH model and its variability according to the reflectance scale factor ( $\alpha_{soil}$ )**

### *2.2.5 Inverse problem configuration*

To understand the contribution of directional information in LAI estimation, the PSH model was inverted by using first one ("A3"), then three ("A2" "A3" "A4") and finally five ("A1" "A2" "A3" "A4" "A5") view angles.

Several researches demonstrated that the optimal information in quantitative characterization of forest canopies (Blackburn, 1998) or vegetation (Broge and Leblanch, 2000) or agricultural crops (Carter, 1998, Thenkabail et al., 2002a) is present in a few specific narrowbands rendering a large number of wavebands redundant. Thus, in order to reduce redundancy and to understand the contribution of the spectral information on the directionality, the experiment was first performed with the full spectral 62 CHRIS bands. Second the process was repeated with a selection of optimal spectral bands in the visible (542, 563, 583, 605, 664, 674 and 694 nm), in the red edge (706, 718, 731, 745 and 758 nm) and in the infrared (773, 780, 831 and 889 nm) part of the spectrum (according to the results of previous works found in literature, Thenkabail, 2004) and finally by using 4 bands close to Landsat-TM spectral configuration.

For each of the experiments, the LAI accuracy is evaluated in terms of root mean square error ($RMSE_{LAI}$) and relative percentage error ($RPE_{LAI}$).

## 2.3 The semi-empirical approach: CLAIR model (LAI-WDVI)

To compare the physical approach with a traditional VI one, the semi-empirical relationship between the Weighted Differences Vegetation Index (WDVI) and LAI (CLAIR model, Clevers, 1989, 0) was adopted.

The CLAIR model (Clevers, 1989) is based on the logarithmic relation between LAI and the WDVI. It assumes that all parameters are constant, except LAI and soil brightness:

$$LAI = -\frac{1}{\alpha^*}\ln\left(1-\frac{WDVI}{WDVI_\infty}\right) \qquad \textbf{Eq. 3}$$

where α* is an extinction coefficient, expressing the increase of LAI for a unitary of WDVI. It has to be estimated from simultaneous measurements of LAI and WDVI. WDVI∞ expresses the asymptotical value of WDVI for LAI $\rightarrow \infty$.

$$WDVI = \rho_i - \rho_r \frac{\rho_{si}}{\rho_{sr}} \qquad \textbf{Eq. 4}$$

where $\rho_i$ and $\rho_r$ indicate the reflectance of the observed canopy in red and infrared bands respectively, while $\rho_{si}$ and $\rho_{sr}$ are the corresponding values for bare soil conditions. The ratio ρsi/ρsr can be taken as constant, in analogy with the "soil line concept" (Baret et al., 1993).

# *Chapter 3*

## 3 Experimental results

### 3.1 Validation of the PSH model

A preliminary model validation was performed comparing a canopy reflectance spectrum acquired by ASD FieldSpec® spectroradiometer over an alfalfa canopy during the field campaign with the spectrum simulated by the PSH model. Parameter values were set as follows: nadir view, $Chl_{a+b}$=57 mg/cm$^2$, $C_w$=0.011 g/cm$^2$, $C_m$=0.0055 g/cm$^2$, LAI=2.7, HOT=0.057 and $E_{SKY}$=0.16, as from ground measurements, while N=1.8 (Walter-Shea et al., 1997) and Spherical LAD (ALA= 57°) were taken from literature.

The model was run with 9 different measured soil spectra during the campaign, ranging from very bright (dry) to very dark (wet), showing a good agreement between measured and all simulated data. Figure 14 shows the best result obtained with a relative percentage error (RPE) of 7.8% using a wet soil reflectance spectrum.

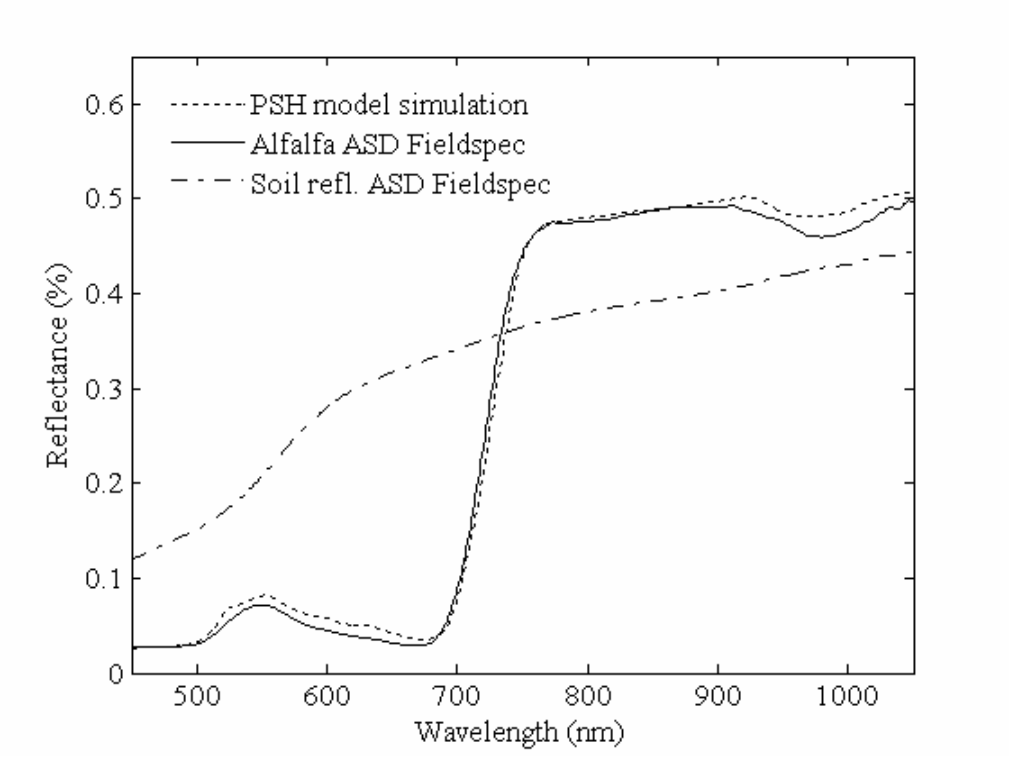


**Figure 14 Field measurement vs. simulated spectra for Alfalfa**

To observe the soil background effect on the canopy reflectance, the PSH model was run by using soil spectra from very bright (dry) to very dark (wet) and different LAI values. In Figure 15 is demonstrated how the soil reflectance influences the spectral response of the surface to a noticeable extent for a LAI value of 1.50 and even for a higher value of 3.0 in the near infrared part of the spectrum.

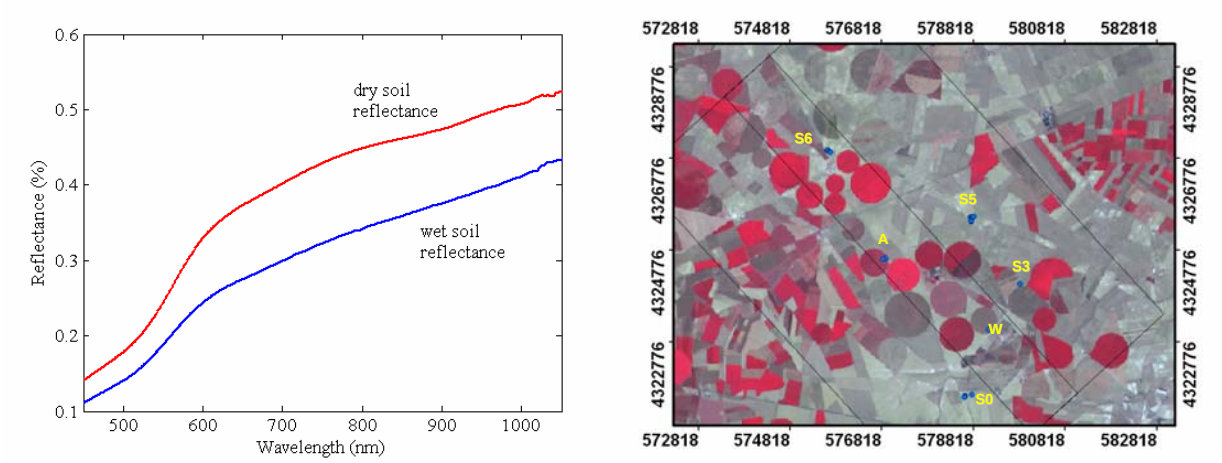


S5:dry soil spot S6:wet soil spot; A:alfalfa

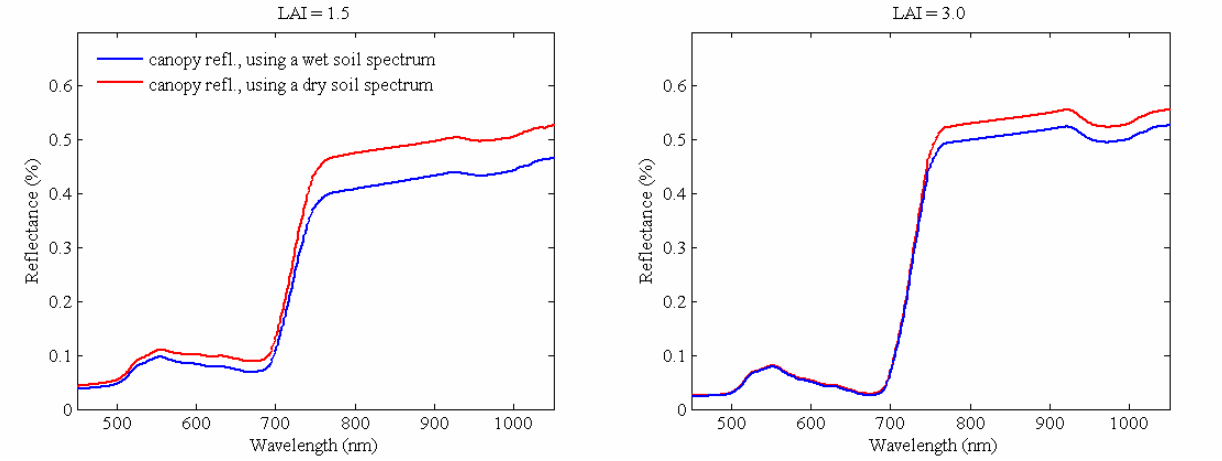


**Figure 15 Canopy reflectance simulated for a low and for an high LAI value by using dry and wet soil spectra as input of PSH model (N=1.8; $Chl_{a+b}$=57 µg/cm$^2$; $C_w$=0.011 g/cm$^2$; $C_m$=0.0055 g/cm$^2$; LAI = 1.5 (left) and 3.0 (right); hot= 0.057; ALA=57°; nadir view; SZA=25°)**

The spectral and angular reflectance of different samples of alfalfa fields was then extracted from CHRIS/PROBA imagery and compared with the simulated ones. The best result was achieved (RPE of 10% over all wavelength and view angles) for an alfalfa sample with LAI value of 1.8 (Figure 16).

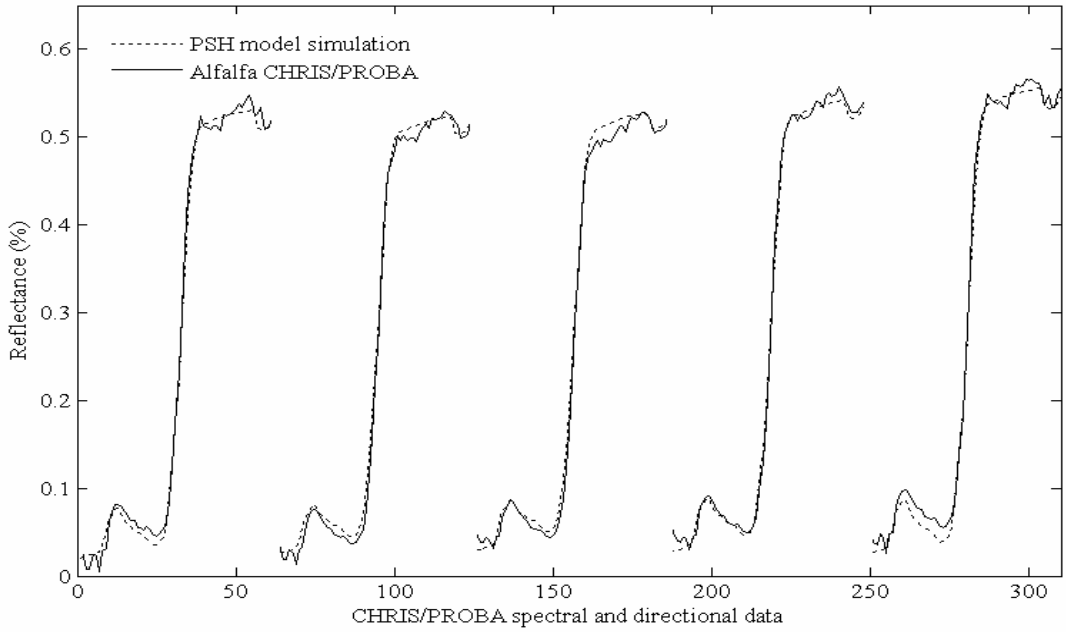


**Figure 16 Alfalfa spectral and directional reflectance. CHRIS/PROBA data vs. forward PSH model simulation**

The green and the near-infrared bands were finally analyzed for all the view angles. A RPE less than 3% for the green band and about 10% for the near-infrared bands was found Figure 17.

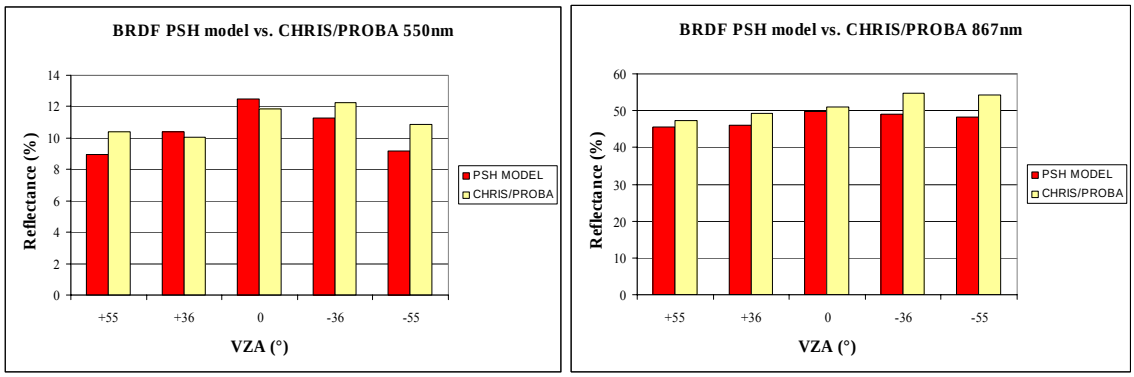


**Figure 17 PSH model test. The models were tested in forward mode in previous studies. Comparison between BRDF model output and CHRIS BRDF sampling showed satisfactory results (D'Urso, 2004). An error less than 3% for the green band and less than 10% for the near-infrared band was found**

A preliminary analysis was also performed for potato stands, using the measured LAI value of 6.2. A quite good accuracy was achieved using as input parameters $Chl_{a+b}$=30 mg/cm$^2$, $C_w$=0.021 g/cm$^2$ $C_m$=0.0046 g/cm$^2$ (from ground measurements), while N=2.0, HOT=0.1 and ALA=27° were assumed from literature. The most relevant discrepancies between model and measurement were

found again in the near-infrared region for the -36° and -55° images (backward viewing direction), while for the red region the model seems to perform more accurately.

### *3.1.1 Conclusions*

A preliminary analysis on CHRIS/PROBA data was carried out. The spectral and space information content of the satellite data was exploited to validate the canopy reflectance model.

The effectiveness of the combined use of PROSPECT and SAILH models could be demonstrated to simulate canopy BRDF of alfalfa crop with an acceptable accuracy. The investigation also showed the importance of the soil reflectance component on the overall spectral reflectance. Therefore a soil reflectance map of the image as well as the removal of the Lambertian surface hypothesis for the bare soil could lead to a more accurate BRDF modelling for sparse canopies. The goodness of the results obtained, at least for the crops under investigation, encouraged the use of these models in the inverse mode in order to retrieve vegetation parameters.

## 3.2 Invertibility of the PSH model

Due to the ill-pose nature of the inverse problem, the invertibility of a canopy reflectance model is not guaranteed (Goel, 1988). Therefore, before PSH model is inverted with real measured reflectance data, it is necessary to test its inversion performance using synthetic model generated error-free data and the selected LM algorithm.

The canopy reflectance for three different parameter sets (X, Y and Z, see Table x) was thus computed by using model inputs representative of those encountered in the field measurement (see section x). The geometric configuration of CHRIS/PROBA respective to the Barrax acquisition was adopted for all the simulations (62 bands and 5 view angles). A Uniform and a Spherical leaf angle distribution were selected with an average leaf inclination of 45° (case: X) and 57° (case: Y). For the Y case, the soil reflectance was varied scaled from dark to wet soil conditions ($\alpha_{soil}$= 0.8) (case: Z). Variations of these three base cases were made by varying LAI values to cover a wide range from 0.8 to 5.4.

Since in an inversion problem, model parameters may be excessively sensitive to reflectance [Goel, 1988], small errors in measured reflectance may result in large errors in retrieved parameters. To take into account this uncertainty, Gaussian noise was added to synthetic reflectance data (cases: Xn,Yn and Zn).

The Relative Root Mean Square Errors ($RRMSE_{LAI}$) and Relative Percentage Errors ($RPE_{LAI}$) for LAI estimation accuracies are shown in Table 4 for all the cases.

| | | case 1 | case 2 | case 3 | case 4 | case 5 | case 6 | Mean |
|---|---|---|---|---|---|---|---|---|
| | LAI: | 0.8 | 1.5 | 2.7 | 3.6 | 4.5 | 5.4 | errors |
| Xn | $RRMSE_{LAI}$ | 0.05 | 0.12 | 0.32 | 0.03 | 0.17 | 0.44 | **0.19** |
| | $RPE_{LAI}$ | 5.7% | 9.7% | 19.3% | 1.6% | 8.2% | 19.1% | **10.6%** |
| Yn | $RRMSE_{LAI}$ | 0.06 | 0.14 | 0.33 | 0.18 | 0.06 | 0.21 | **0.16** |
| | $RPE_{LAI}$ | 6.2% | 11.3% | 19.9% | 9.4% | 2.7% | 9.2% | **9.8%** |
| Zn | $RRMSE_{LAI}$ | 0.06 | 0.14 | 0.31 | 0.46 | 0.13 | 0.27 | **0.23** |
| | $RPE_{LAI}$ | 7.1% | 11.3% | 19.1% | 24.5% | 6.1% | 11.6% | **13.3%** |

**Table 4 $RRMSE_{LAI}$ and $RPE_{LAI}$ . Xn: ALA=47°; Yn: ALA=57°; Zn: ALA=57° & very dark soil input**

The $RRMSE_{ALA}$ and $RPE_{ALA}$ for ALA estimation accuracies are shown in Table 5 for all the cases.

| | | case 1 | case 2 | case 3 | case 4 | case 5 | case 6 | Mean |
|---|---|---|---|---|---|---|---|---|
| | LAI: | 0.8 | 1.5 | 2.7 | 3.6 | 4.5 | 5.4 | errors |
| Xn | $RRMSE_{ALA}$ | 0.36 | 0.39 | 0.16 | 0.05 | 0.11 | 0.09 | **0.19** |
| | $REP_{ALA}$ | 5.3% | 5.8% | 2.5% | 0.8% | 1.7% | 1.3% | **2.9%** |
| Yn | $RRMSE_{ALA}$ | 0.19 | 0.38 | 0.34 | 0.06 | 0.10 | 0.01 | **0.18** |
| | $REP_{ALA}$ | 2.5% | 5.0% | 4.5% | 0.7% | 1.3% | 0.1% | **2.4%** |
| Zn | $RRMSE_{ALA}$ | 0.16 | 0.21 | 0.11 | 0.01 | 0.07 | 0.03 | **0.10** |
| | $REP_{ALA}$ | 2.2% | 2.8% | 1.5% | 0.1% | 1.0% | 0.4% | **1.3%** |

**Table 5 $RRMSE_{ALA}$ and $RPE_{ALA}$ . Xn: ALA=47°; Yn: ALA=57°; Zn: ALA=57° & very dark soil input**

Model input parameters are shown in Table 6 and Table 7 for the X and Y cases (ALA 45° and 57°), respectively. The estimated parameters are called "Estimated a and b", i.e. noise-free and with a relative 10 % Gaussian noise added, respectively. Model input parameters for the case Y (dark soil) are shown in Table 8.

### *3.2.1 Conclusions*

By using LM optimization algorithm and the parameterization as in Table 3, the invertibility of the PSH model was shown for typical conditions using noise-free synthetic data generated under satellite sampling schemes. In general, LAI estimates were reasonably accurate ($RPE_{LAI}$=10%) except for case 3 were the mean $RPE_{LAI}$ is 19.4%. ALA was more accurately estimated with a mean percentage error of 2.2%. The PROSPECT parameters were estimated within a mean percentage error of 30%, 24% and 5% for $C_w$, $C_m$ and $Chl_{a+b}$, respectively. The N parameter was

always not estimated. The hot parameter was retrieved with large errors probably due to the small sensitivity of this parameter when the sensor-target-sun positions are not in the principal plain configuration as for the CRHIS/PROBA orbit. Soil reflectance was systematically slightly overestimated. Effects of random Gaussian noise in synthetic data were also tested and parameters estimation remained accurate. In Figure 18 the synthetic noise-added reflectance (•) is plotted (obtained running PSH model in forward mode) and the corresponding retrieved reflectance (■) by PSH model inversion. The model input and the parameter estimates are shown Table 6, case 3.

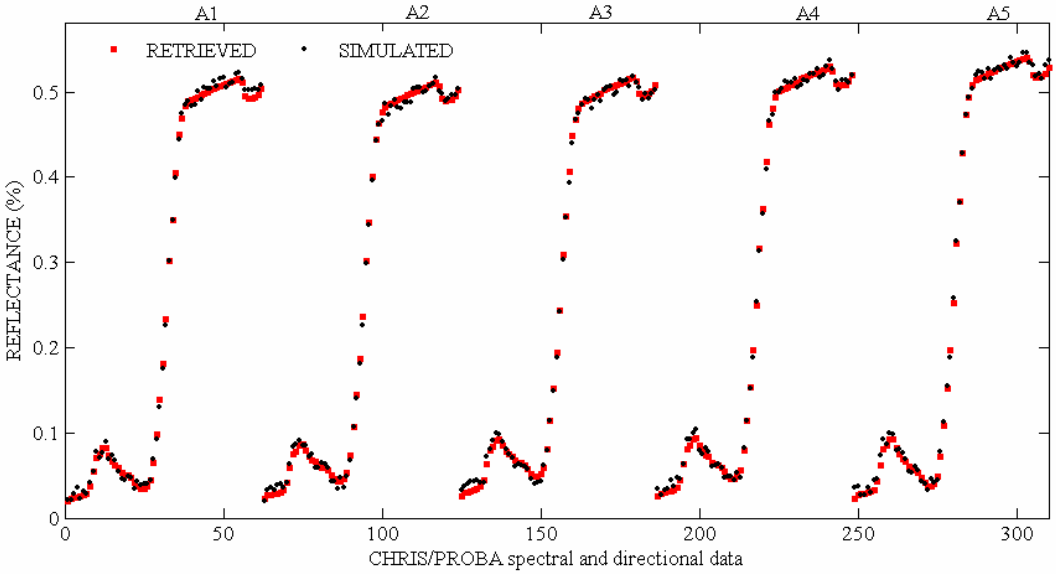


**Figure 18 Data fitting of synthetic noise-added reflectance (•) (obtained running PSH model in forward mode for LAI = 2.70) and the corresponding retrieved reflectance (■) by PSH model inversion.**

| Model parameters | Input **case 1** | - | Estimated a | b | Input **case 2** | - | Estimated a | b |
|---|---|---|---|---|---|---|---|---|
| N | 1.80 | | 1.86 | 2.00 | 1.80 | | 1.87 | 2.00 |
| $Chl_{a+b}$ | 66 | | 66 | 68 | 66 | | 66 | 69 |
| $C_w$ | 0.011 | | 0.015 | 0.015 | 0.011 | | 0.015 | 0.015 |
| $C_m$ | 0.0055 | | 0.0071 | 0.0067 | 0.0055 | | 0.0067 | 0.0060 |
| LAI | **0.80** | | 0.82 | 0.75 | **1.50** | | 1.53 | 1.35 |
| HOT | 0.250 | | 0.166 | 0.173 | 0.250 | | 0.183 | 0.182 |
| ALA | 45.0 | | 45.6 | 42.6 | 45.0 | | 45.9 | 42.4 |
| $\alpha_{soil}$ | 1 | | 1.034 | 1.043 | 1 | | 1.072 | 1.067 |

| Model parameters | Input **case 3** | - | Estimated a | b | Input **case 4** | - | Estimated a | b |
|---|---|---|---|---|---|---|---|---|
| N | 1.80 | | 1.91 | 2.00 | 1.80 | | 1.94 | 1.80 |
| $Chl_{a+b}$ | 66 | | 67 | 68 | 66 | | 67 | 70 |
| $C_w$ | 0.011 | | 0.015 | 0.015 | 0.011 | | 0.015 | 0.015 |
| $C_m$ | 0.0055 | | 0.0057 | 0.0049 | 0.0055 | | 0.0050 | 0.0075 |
| LAI | **2.70** | | 2.51 | 2.18 | **3.60** | | 2.98 | 3.54 |
| HOT | 0.250 | | 0.173 | 0.199 | 0.250 | | 0.182 | 0.785 |
| ALA | 45.0 | | 45.3 | 43.9 | 45.0 | | 45.6 | 45.4 |
| $\alpha_{soil}$ | 1 | | 1.142 | 1.137 | 1 | | 1.2 | 1.061 |

| Model parameters | Input **case 5** | - | Estimated a | b | Input **case 6** | - | Estimated a | b |
|---|---|---|---|---|---|---|---|---|
| N | 1.80 | | 1.80 | 1.80 | 1.80 | | 1.80 | 1.80 |
| $Chl_{a+b}$ | 66 | | 70 | 70 | 66 | | 70 | 70 |
| $C_w$ | 0.011 | | 0.015 | 0.015 | 0.011 | | 0.015 | 0.015 |
| $C_m$ | 0.0055 | | 0.0059 | 0.0073 | 0.0055 | | 0.0060 | 0.0068 |
| LAI | **4.50** | | 3.83 | 4.13 | **5.40** | | 4.35 | 4.37 |
| HOT | 0.250 | | 0.39 | 0.974 | 0.250 | | 0.476 | 1 |
| ALA | 45.0 | | 44.6 | 45.8 | 45.0 | | 44.7 | 44.4 |
| $\alpha_{soil}$ | 1 | | 1.15 | 1.158 | 1 | | 1.2 | 1.2 |

**Table 6 Model input parameter for base case X varying the LAI and estimated parameter for noise-free reflectance (a) and noise-added reflectance (b)**

| Model parameters | Input **case 1** | - | Estimated a | b | Input **case 2** | - | Estimated a | b |
|---|---|---|---|---|---|---|---|---|
| N | 1.80 | | 1.91 | 2.00 | 1.80 | | 1.94 | 2.00 |
| $Chl_{a+b}$ | 66 | | 67 | 67 | 66 | | 67 | 70 |
| $C_w$ | 0.011 | | 0.015 | 0.015 | 0.011 | | 0.015 | 0.015 |
| $C_m$ | 0.0055 | | 0.0067 | 0.0060 | 0.0055 | | 0.0063 | 0.0055 |
| LAI | **0.80** | | 0.81 | 0.75 | **1.50** | | 1.51 | 1.33 |
| HOT | 0.250 | | 0.055 | 0.056 | 0.250 | | 0.112 | 0.126 |
| ALA | 57.0 | | 57.2 | 55.6 | 57.0 | | 57.4 | 54.2 |
| $\alpha_{soil}$ | 1 | | 1.028 | 1.039 | 1 | | 1.056 | 1.045 |

| Model parameters | Input **case 3** | - | Estimated a | b | Input **case 4** | - | Estimated a | b |
|---|---|---|---|---|---|---|---|---|
| N | 1.80 | | 1.95 | 2.00 | 1.80 | | 1.92 | 1.80 |
| $Chl_{a+b}$ | 66 | | 68 | 70 | 66 | | 69 | 70 |
| $C_w$ | 0.011 | | 0.015 | 0.015 | 0.011 | | 0.015 | 0.015 |
| $C_m$ | 0.0055 | | 0.0056 | 0.0045 | 0.0055 | | 0.0052 | 0.0061 |
| LAI | **2.70** | | 2.53 | 2.16 | **3.60** | | 3.13 | 3.26 |
| HOT | 0.250 | | 0.147 | 0.159 | 0.250 | | 0.183 | 0.623 |
| ALA | 57.0 | | 56.4 | 54.4 | 57.0 | | 56.4 | 56.6 |
| $\alpha_{soil}$ | 1 | | 1.085 | 1.07 | 1 | | 1.107 | 1 |

| Model parameters | Input **case 5** | - | Estimated a | b | Input **case 6** | - | Estimated a | b |
|---|---|---|---|---|---|---|---|---|
| N | 1.80 | | 1.80 | 1.80 | 1.80 | | 1.80 | 1.80 |
| $Chl_{a+b}$ | 66 | | 70 | 70 | 66 | | 70 | 70 |
| $C_w$ | 0.011 | | 0.015 | 0.015 | 0.011 | | 0.015 | 0.015 |
| $C_m$ | 0.0055 | | 0.0055 | 0.0069 | 0.0055 | | 0.0056 | 0.0068 |
| LAI | **4.50** | | 3.84 | 4.38 | **5.40** | | 4.45 | 4.90 |
| HOT | 0.250 | | 0.316 | 1 | 0.250 | | 0.38 | 1 |
| ALA | 57.0 | | 56.1 | 57.8 | 57.0 | | 56.3 | 56.9 |
| $\alpha_{soil}$ | 1 | | 1.097 | 1.036 | 1 | | 1.139 | 1.107 |

**Table 7 Model input parameter for base case Y varying the LAI and estimated parameter for noise-free reflectance (a) and noise-added reflectance (b)**

| Model parameters | Input **case 1** | - | Estimated a | b | Input **case 2** | - | Estimated a | b |
|---|---|---|---|---|---|---|---|---|
| N | 1.80 | | 1.90 | 2.00 | 1.80 | | 1.91 | 2.00 |
| $Chl_{a+b}$ | 66 | | 67 | 67 | 66 | | 66 | 68 |
| $C_w$ | 0.011 | | 0.015 | 0.015 | 0.011 | | 0.015 | 0.015 |
| $C_m$ | 0.0055 | | 0.0066 | 0.0054 | 0.0055 | | 0.0063 | 0.0047 |
| LAI | **0.80** | | 0.81 | 0.74 | **1.50** | | 1.53 | 1.33 |
| HOT | 0.250 | | 0.056 | 0.006 | 0.250 | | 0.127 | 0.106 |
| ALA | 57.0 | | 57.4 | 55.8 | 57.0 | | 57.8 | 55.4 |
| $\alpha_{soil}$ | 0.8 | | 0.825 | 0.838 | 0.8 | | 0.852 | 0.852 |

| Model parameters | Input **case 3** | - | Estimated a | b | Input **case 4** | - | Estimated a | b |
|---|---|---|---|---|---|---|---|---|
| N | 1.80 | | 1.87 | 2.00 | 1.80 | | 1.80 | 2.00 |
| $Chl_{a+b}$ | 66 | | 67 | 68 | 66 | | 68 | 67 |
| $C_w$ | 0.011 | | 0.015 | 0.015 | 0.011 | | 0.015 | 0.015 |
| $C_m$ | 0.0055 | | 0.0056 | 0.0040 | 0.0055 | | 0.0055 | 0.0039 |
| LAI | **2.70** | | 2.62 | 2.18 | **3.60** | | 3.30 | 2.72 |
| HOT | 0.250 | | 0.196 | 0.176 | 0.250 | | 0.279 | 0.231 |
| ALA | 57.0 | | 57.7 | 56.1 | 57.0 | | 57.3 | 56.9 |
| $\alpha_{soil}$ | 0.8 | | 0.896 | 0.909 | 0.8 | | 0.917 | 0.973 |

| Model parameters | Input **case 5** | - | Estimated a | b | Input **case 6** | - | Estimated a | b |
|---|---|---|---|---|---|---|---|---|
| N | 1.80 | | 1.80 | 1.80 | 1.80 | | 1.80 | 1.80 |
| $Chl_{a+b}$ | 66 | | 70 | 70 | 66 | | 70 | 70 |
| $C_w$ | 0.011 | | 0.015 | 0.015 | 0.011 | | 0.015 | 0.015 |
| $C_m$ | 0.0055 | | 0.0057 | 0.0068 | 0.0055 | | 0.0057 | 0.0067 |
| LAI | **4.50** | | 3.97 | 4.23 | **5.40** | | 4.55 | 4.77 |
| HOT | 0.250 | | 0.366 | 1 | 0.250 | | 0.425 | 1 |
| ALA | 57.0 | | 56.7 | 57.6 | 57.0 | | 56.8 | 56.8 |
| $\alpha_{soil}$ | 0.8 | | 0.929 | 0.864 | 0.8 | | 1 | 0.955 |

**Table 8 Model input parameter for base case Z varying the LAI and estimated parameter for noise-free reflectance (a) and noise-added reflectance (b)**

3.3 Optimization and analysis of the inversion procedure.

After performing a preliminary analysis of the invertibility of PSH model both on error free and noise-added data, the inversion algorithm was further investigated. In next section a more mathematical view of the problem is given. The minimum of the cost function value, the number of cost function evaluations and the inversion time are considered.

The canopy reflectance was computed by using PSH model in forward mode for three different LAI values (0.5, 3.0 and 5.0). The other parameters were considered fixed, described in Table 9 (forward simulation).

| Model parameters | N | $Chl_{a+b}$ | $C_w$ | $C_m$ | LAI | ALA | HOT | $\alpha_{soil}$ |
|---|---|---|---|---|---|---|---|---|
| Forward simulation | 1.8 | 50 | 0.011 | 0.0055 | *var.* | 57 | 0.0057 | 1.0 |
| Lower bound - (LB) | 1.3 | 30 | 0.011 | 0.001 | 0.01 | 30 | 0.001 | 0.8 |
| Upper bound - (UB) | 2.0 | 70 | 0.1 | 0.01 | 6.00 | 80 | 1.000 | 1.2 |

**Table 9 Set of PSH model parameters used in forward simulation and Lower and Upper bounds for the same parameters used in inverse simulations.**

The influence of starting off the inversion process from different initial parameter values was tested, first by using as initial values the set of parameters used in forward model simulation except for LAI parameter, that was set up equal to 3.0 (when LAI=0.5 and LAI=5) and to 1.5 (when LAI=3.0) and then by using lower and upper bounds parameter values, LB and UB respectively. In Table 10 estimations of LAI ($LAI_{est}$) from inverting model-generated data are presented, first for 62 and then for 4 spectral bands and 5 view directions.

| | | **62 bands – 5 view directions** | | | | **4 bands – 5 view directions** | | | |
|---|---|---|---|---|---|---|---|---|---|
| *for:* | Initial values | $LAI_{est}$ | f-count | Time | min f(x) | $LAI_{est}$ | f-count | Time | min f(x) |
| **LAI=0.5** | *LAI 3.0* | 0.49 | 403 | 103 | $6*10^{-6}$ | 0.50 | 327 | 66 | $4*10^{-4}$ |
| | *LB* | 0.50 | 404 | 102 | $1*10^{-5}$ | 0.50 | 533 | 108 | $4*10^{-6}$ |
| | *UB* | 0.49 | 848 | 205 | 0.4 | 0.49 | 318 | 65 | $2*10^{-3}$ |
| | | $LAI_{est}$ | f-count | Time | min f(x) | $LAI_{est}$ | f-count | Time | min f(x) |
| **LAI=3.0** | *LAI 1.5* | 3.00 | 347 | 80 | $6*10^{-5}$ | 3.00 | 409 | 81 | $2*10^{-4}$ |
| | *LB* | 2.99 | 363 | 92 | $5*10^{-4}$ | 2.78 | 426 | 87 | 0.0027 |
| | *UB* | 3.00 | 558 | 141 | $1*10^{-6}$ | 2.77 | 459 | 93 | 0.0033 |
| | | $LAI_{est}$ | f-count | Time | min f(x) | $LAI_{est}$ | f-count | Time | min f(x) |
| **LAI=5.0** | *LAI 3.0* | 5.00 | 518 | 134 | $2*10^{-6}$ | 4.03 | 402 | 84 | 0.012 |
| | *LB* | 4.99 | 895 | 232 | $2*10^{-6}$ | 4.76 | 447 | 89 | $8*10^{-4}$ |
| | *UB* | 5.00 | 607 | 157 | $2*10^{-6}$ | 5.60 | 517 | 106 | $7*10^{-4}$ |

**Table 10 LAI estimates ($LAI_{est}$) for three LAI forward simulations (0.5, 3.0 and 5.0) by using 62 and 4 spectral bands. The optimization process starts from different initial parameter values. In the table is also shown the number of cost function evaluations (f-count), the optimization time in seconds (Time) and the minimum of the cost function f(x).**

For **LAI** values of **0.5**, the inversion results showed in general a good accuracy for LAI estimation. When exploiting 62 spectral bands and 4 spectral bands, the cost function values are on the order of $10^{-5}$, except when the inversion process is started from the upper bounds for 62 bands. In this case, the optimization is probably stacked in a local minimum due to the counterbalancing effect of the other parameters. The cost function showed a high value (min. of f(x)=0.4) despite the good accuracy in estimating LAI (LAI=0.49). An alternative inversion parameterization was thus tested, restarting the optimization by using as initial values not the UB but the set of parameters estimated from the previous optimization. The retrieved LAI was 0.49 with a new minimum of the cost function of $7*10^{-6}$. In this case, the starting points seem to play a crucial role and restarting the optimization generates good approximation.

For **LAI=3.0** and **LAI=5.0**, the results are only accurate in terms of min f(x) and $LAI_{est}$ when the full spectral information is exploited in the inversion of the PSH model. This might be caused by a lower sensitivity of the model to higher LAI values,

The relevance of using 62 or 4 bands and the effect of searching for a low or high LAI is shown in Figure 19 and Figure 20. The error surface for LAI and ALA parameters are plotted considering a cost function based on 62 or 4 bands, respectively.

The error surface is relatively sharp and well-behaved for low LAI (LAI<2) and when more spectral information is provided. It becomes flat for high LAI values and exploiting 4 bands.

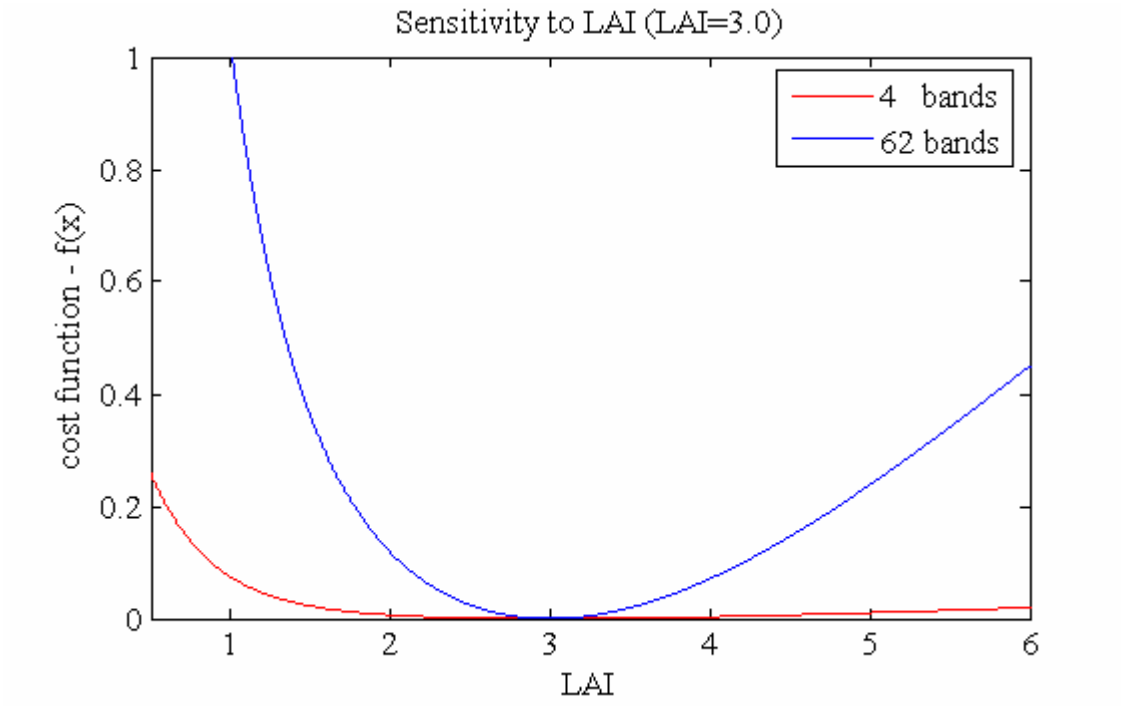


**Figure 19 Sensitivity of the cost function to LAI for LAI=3.0 considering 62 and 4 spectral bands and 5 view directions**

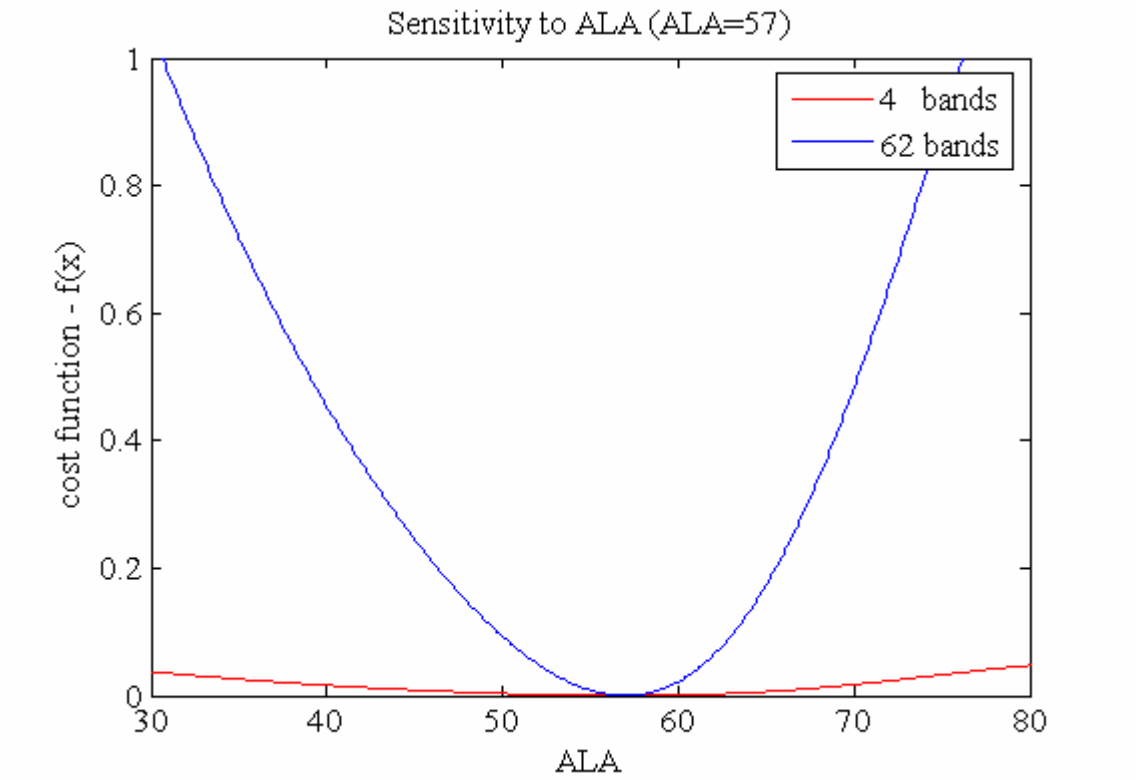


**Figure 20 Sensitivity of the cost function to ALA for ALA=57 and LAI=3.0 considering 62 and 4 spectral bands and 5 view directions**

Since the largest uncertainties in parameter estimation were observed for LAI=5.0 and 4 spectral bands, the influence of different model inversion parameterizations and data set up was considered for these cases.

The first analysis was performed to understand the influence of initial parameter values on the optimization. The inversion was run starting from standard initial parameter values. At the end of the first run a condition on the cost function was set up: if f(x) is less or equal to a defined minimum value, the optimization is stopped and the results are displayed; if f(x) is greater than the minimum, the optimization is restarted by using as initial values the set of parameters estimated from the previous optimization. In this case the effect of not appropriate starting point should be eliminated.

A second alternative was tested reducing the free parameters to be retrieved by model inversion. First $C_w$ and $C_m$ were kept fixed, and then the experiment was repeated for ALA and $\alpha_{soil}$ parameters. The results are shown in Table 11.

In the latter case, restarting the optimization does not bring any improvement. While reducing the number of free parameters, it is still possible to obtain LAI with a good accuracy by exploiting only 4 bands. On the one hand, it is possible to get the best result, in terms of cost function, fixing

ALA and $\alpha_{soil}$. On the other hand, from an operative point of view it seems more feasible to fix $C_w$ and $C_m$ since these are parameters possible to measure or to approximate with a-*priori* knowledge. However, ALA and $\alpha_{soil}$ are more difficult to determinate.

| | | 4 bands | | | | other parameter estimated | | | | | | |
|---|---|---|---|---|---|---|---|---|---|---|---|---|
| | | $LAI_{est}$ | f-count | Time | min f(x) | N | Chla+b | Cw | Cm | ALA | HOT | $\alpha_{soil}$ |
| **LAI=5.0** | UB **restarting** | 5.60 | 599 | 118 | $6*10^{-4}$ | 1.78 | 50.56 | 0.011 | 0.0057 | 56.01 | 0.046 | 0.829 |
| | UB **Cw & Cm fixed** | 5.06 | 722 | 145 | $4*10^{-5}$ | 1.80 | 50.25 | **0.011** | **0.0055** | 56.65 | 0.054 | 0.966 |
| | UB **ALA & $\alpha_{soil}$ fixed** | 4.99 | 545 | 109 | $8*10^{-7}$ | 1.79 | 50.03 | 0.013 | 0.0055 | **57.00** | 0.058 | **1.00** |

**Table 11 Alternative approaches of model inversion parameterizations and results.**

The sensitivity of the cost function to $C_w$ and $C_m$ is plotted in Figure 21 and Figure 22, respectively.

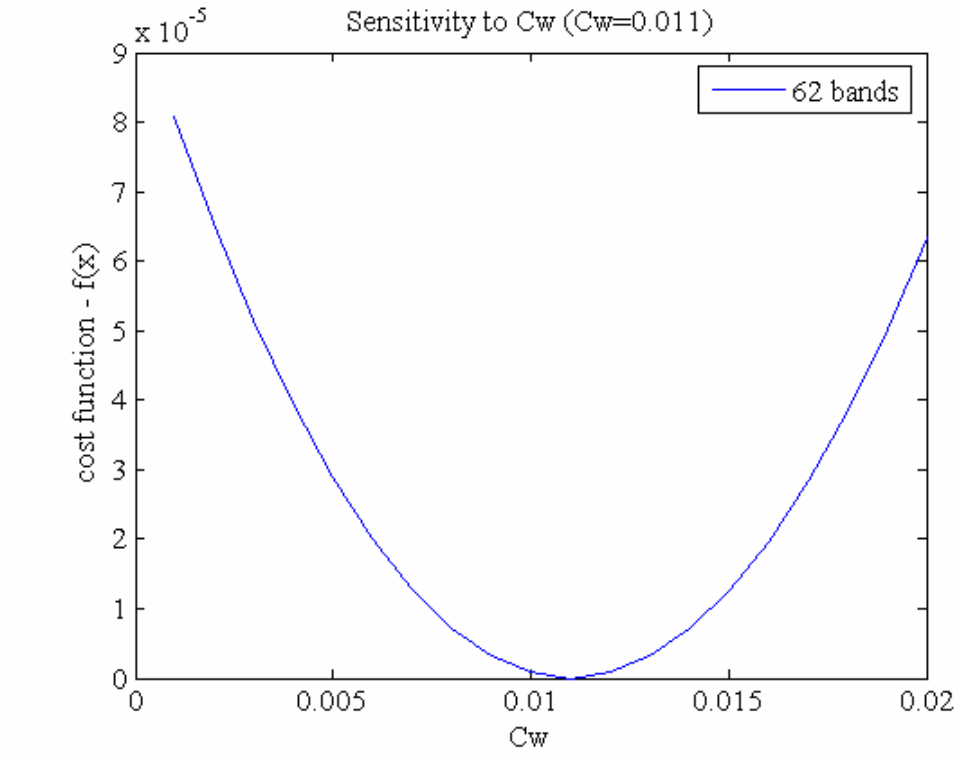


**Figure 21 Sensitivity of the cost function to Cw for Cw=0.011 considering 62 spectral bands and 5 view directions**

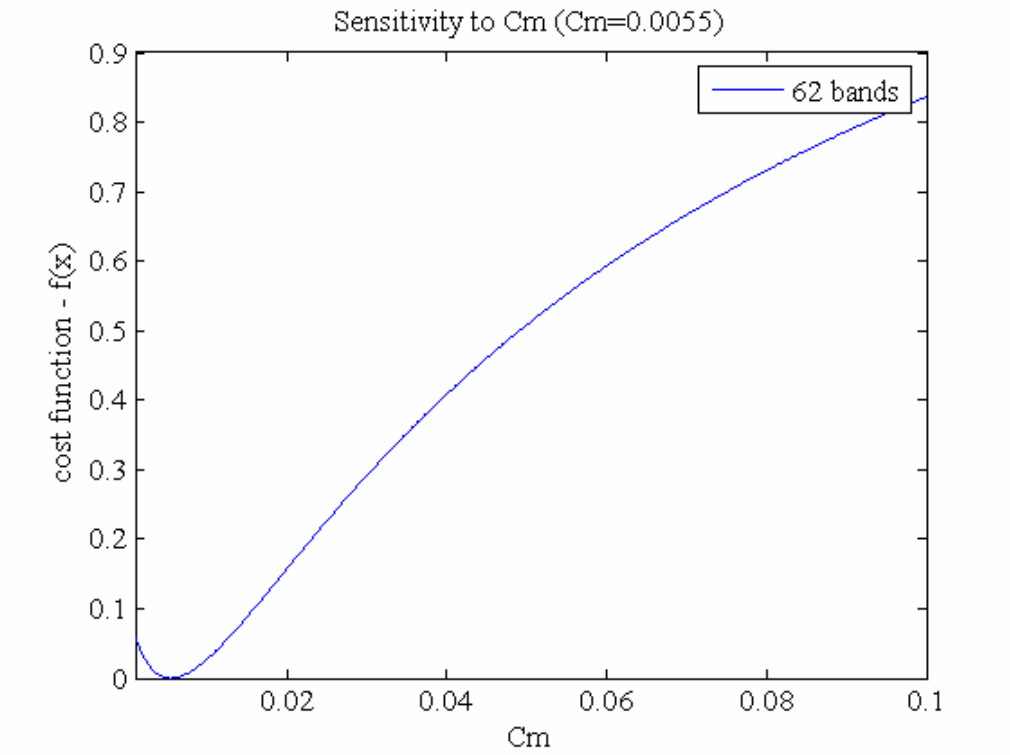


**Figure 22 Sensitivity of the cost function to Cm, for Cm=0.0055 considering 62 spectral bands and 5 view directions**

Finally, the inversion was repeated by using 16 bands selected as reported in section 2.2.5. The results are shown in Table 12 for LAI=5.0, starting the optimization from the lower and the upper bounds. The estimated LAI, the cost function value and the inversion time, all indicate that some of the problems reported before by using only 4 spectral bands can be avoid adding spectral information until at a certain point, after that it starts to be redundant.

| | | **16 bands – 5 view directions** | | | | Values of other parameters estimated: | | | | | | |
|---|---|---|---|---|---|---|---|---|---|---|---|---|
| | | $LAI_{est}$ | f-count | Time | min f(x) | N | $Chl_{a+b}$ | Cw | Cm | ALA | HOT | $\alpha_{soil}$ |
| **LAI=5.0** | *LB* | 5.12 | 475 | 99 | $7*10^{-4}$ | 1.78 | 50.29 | 0.011 | 0.0056 | 56.67 | 0.058 | 0.959 |
| | *UB* | 5.00 | 758 | 161 | $2*10^{-6}$ | 1.80 | 50.00 | 0.011 | 0.0055 | 56.98 | 0.057 | 0.998 |

**Table 12 LAI estimation accuracy for LAI=5 by using 16 bands and 5 view directions.**

The directional information was finally analyzed. The inversions were performed again for the three LAI values by using only one view angle. The results are shown in Table 12.

| | | **62 bands - 1 view angle** | | | |
|---|---|---|---|---|---|
| *For:* | | $LAI_{est}$ | f-count | Time | min f(x) |
| *LAI=0.5* | **LAI 3** | 0.38 | 78 | 48 | 0.0015 |
| *LAI=3.0* | **LAI 1.5** | 2.54 | 73 | 35 | 0.043 |
| *LAI=5.0* | **LAI 3** | 6.00 | 932 | 51 | 0.0683 |

**Table 13 LAI estimation accuracy for LAI=0.5, LAI=3.0 and LAI=5.0 by using 62 bands and 1 view direction**

## 3.4 Inversion results

LAI root mean square error ($RMSE_{LAI}$) and relative percentage error ($RPE_{LAI}$) trend is reported in Table 14, Table 15, and Table 16 for alfalfa, corn and potato, respectively.

| *Alfalfa* | | *Directional* | | | |
|---|---|---|---|---|---|
| | | 1 | 3 | 5 | Angles |
| *Spectral* | 4 | 24.5% | 23.1% | 18.5% | |
| | 16 | 25.6% | 25.7% | 21.1% | |
| | 62 | 24.4% | 25.3% | 18.8% | |
| | Bands | | | | $RPE_{LAI}$ |
| | | *Directional* | | | |
| | | 1 | 3 | 5 | Angles |
| *Spectral* | 4 | 0.71 | 0.49 | 0.44 | |
| | 16 | 0.82 | 0.61 | 0.49 | |
| | 62 | 0.76 | 0.59 | 0.41 | |
| | Bands | | | | $RMSE_{LAI}$ |

**Table 14 LAI root mean square error ($RMSE_{LAI}$) and relative percentage error ($RPE_{LAI}$) trend for alfalfa**

| *Corn* | | *Directional* | | | |
|---|---|---|---|---|---|
| | | 1 | 3 | 5 | Angles |
| *Spectral* | 4 | 38.4% | 32.9% | 30.6% | |
| | 16 | 41.1% | 14.1% | 14.0% | |
| | 62 | 31.4% | 13.1% | 12.9% | |
| | Bands | | | | $RPE_{LAI}$ |
| | | *Directional* | | | |
| | | 1 | 3 | 5 | Angles |
| *Spectral* | 4 | 1.42 | 1.31 | 1.25 | |
| | 16 | 1.57 | 0.54 | 0.58 | |
| | 62 | 0.76 | 0.59 | 0.41 | |
| | Bands | | | | $RMSE_{LAI}$ |

**Table 15 LAI root mean square error ($RMSE_{LAI}$) and relative percentage error ($RPE_{LAI}$) trend for corn**

| *Potato* | | *Directional* | | | |
|---|---|---|---|---|---|
| | | 1 | 3 | 5 | Angles |
| *Spectral* | 4 | 59.8% | 59.3% | 58.3% | |
| | 16 | 64.3% | 61.5% | 57.5% | |
| | 62 | 64.5% | 62.9% | 55.3% | |
| | Bands | | | | $\boldsymbol{RPE_{LAI}}$ |
| | | *Directional* | | | |
| | | 1 | 3 | 5 | Angles |
| *Spectral* | 4 | 3.21 | 3.18 | 3.14 | |
| | 16 | 3.45 | 3.29 | 3.10 | |
| | 62 | 3.46 | 3.37 | 2.98 | |
| | Bands | | | | $\boldsymbol{RMSE_{LAI}}$ |

**Table 16 LAI root mean square error ($RMSE_{LAI}$) and relative percentage error ($RPE_{LAI}$) trend for potato**

Going from left to right, in each table the $RMSE_{LAI}$ and $RPE_{LAI}$ values were shown corresponding to one angle ("A3"), three angles ("A1","A3", "A5") and five angles ("A1","A2", "A3", "A4" and "A5").

From up to down the values corresponding to 4 (LANDSAT-TM5 configuration), 16 (542, 563, 583, 605, 664, 674, 694, 706, 718, 731, 745, 758, 773, 780, 831 and 889 nm) and 62 (full CHRIS data set) spectral bands are demonstrated.

In case of alfalfa and even more of corn, the LAI estimation accuracy improves for each fixed spectral configuration by adding directional information. However, for each fixed directional configuration, the addition of spectral information does not improve LAI estimation accuracy for alfalfa. Whereas, in case of corn there is a remarkable increase in estimation accuracy going from 4 to 16 spectral bands, but less evident going from 16 to 62 spectral bands. Considering these results, the contribution of directional information seems to be more marked for the estimation performance of LAI than the spectral content.

Concerning the LAI accuracy analysis of potato crops, results indicate the impossibility to achieve reasonable values by using model inversion. Looking at field book notes and photos, reasons may be related to the agronomic practices of growing potato: during the satellite overpass the potato field revealed deep grooves, partly filled with water. Perhaps additional restrictions on the soil reflectance should be considered in the model inversion parameterization. From these results and considerations, a further model analysis was carried out to take into account the effect of the soil background. According to CHRIS/PROBA geometric configuration and the results achieved for potato, two different spectra were simulated by using first as model input a LAI value as estimated from model inversion for the potato fields (mean LAI = 3.1) and then a LAI value as expected from field measurements (mean LAI = 5.3). The effect of the soil influence was simulated, first by using a standard spectrum (in this case LAI = 3) and second a dark soil spectrum with a LAI value of 5.

In Figure 23 an example of the forward modelling results is demonstrated. As observed by several studies for other parameter combinations (see LAI and ALA), a counterbalancing effect of model parameters on the spectral and directional data was also found here between the LAI and the soil brightness.

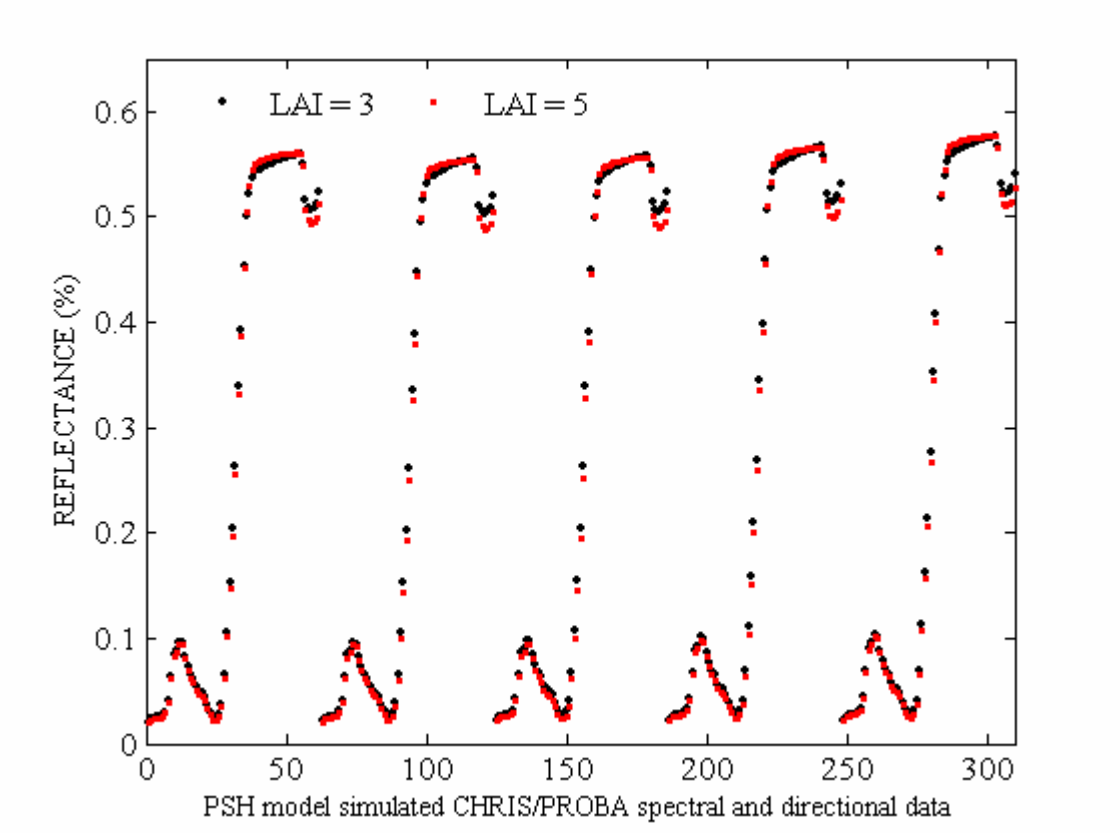


**Figure 23 Different for standard and very wet soil. N=1.5; Chla+b=40; Cw=0.02; Cm0.004 ALA=40**

## 3.5 Validation of model inversion results by using Genetic Algorithms

As discussed in the first part of this work, there are several kinds of optimization routines that can be exploited to numerically invert a canopy reflectance model. The results achieved might be variable depending on the optimization methodology and the inversion parameterization. With the aim to validate the results obtained by using a L-M optimization algorithm, a genetic algorithm was implemented to locate the minimum of the cost function.

The experiment was carried out by exploiting the directional information (from 1 to 5 angles) as well as the spectral information: starting from the simplest configuration (4 bands) to the full spectra (62 bands), by adding at every step the same amount of bands in the visible part and infrared region.

The results for alfalfa and corn (shown in Table 17) confirmed the predominant role of directional information compared to spectral information in the estimation of LAI.

| | *Bands* | | | | | | | | | | |
|---|---|---|---|---|---|---|---|---|---|---|---|
| *Angles* | **4** | **8** | **12** | **16** | **20** | **24** | **28** | **32** | **42** | **62** | |
| **1** | 0.81 | 0.83 | 0.88 | 0.91 | 0.91 | 0.94 | 0.92 | 0.93 | 0.95 | 0.95 | |
| **2** | 0.82 | 0.79 | 0.86 | 0.78 | 0.74 | 0.80 | 0.74 | 0.80 | 0.80 | 0.75 | Alfalfa |
| **3** | 0.73 | 0.74 | 0.75 | 0.76 | 0.76 | 0.79 | 0.76 | 0.78 | 0.78 | 0.76 | |
| **4** | 0.48 | 0.56 | 0.57 | 0.43 | 0.43 | 0.41 | 0.42 | 0.41 | 0.41 | 0.42 | |
| **5** | 0.48 | 0.45 | 0.44 | 0.43 | 0.42 | 0.42 | 0.41 | 0.42 | 0.39 | 0.39 | |
| **1** | 0.74 | 0.94 | 1.09 | 1.14 | 1.22 | 1.17 | 1.11 | 1.20 | 1.18 | 1.26 | |
| **2** | 0.66 | 0.78 | 0.82 | 1.01 | 1.09 | 0.94 | 0.95 | 0.93 | 0.96 | 1.06 | Corn |
| **3** | 0.42 | 0.46 | 0.47 | 0.52 | 0.57 | 0.50 | 0.51 | 0.55 | 0.53 | 0.48 | |
| **4** | 0.51 | 0.38 | 0.41 | 0.49 | 0.54 | 0.46 | 0.48 | 0.49 | 0.44 | 0.40 | |
| **5** | 0.49 | 0.38 | 0.42 | 0.49 | 0.53 | 0.43 | 0.45 | 0.48 | 0.45 | 0.40 | |
| **1** | 3.51 | 3.66 | 3.61 | 3.58 | 3.69 | 3.66 | 3.68 | 3.70 | 3.62 | 3.68 | |
| **2** | 3.52 | 3.63 | 3.64 | 3.65 | 3.72 | 3.70 | 3.71 | 3.72 | 3.66 | 3.64 | Potato |
| **3** | 3.62 | 3.71 | 3.70 | 3.64 | 3.62 | 3.68 | 3.62 | 3.62 | 3.52 | 3.44 | |
| **4** | 3.55 | 3.63 | 3.62 | 3.58 | 3.55 | 3.58 | 3.57 | 3.58 | 3.45 | 3.37 | |
| **5** | 3.50 | 3.54 | 3.51 | 3.41 | 3.49 | 3.46 | 3.46 | 3.49 | 3.41 | 3.28 | |

**Table 17 RMSE values obtained by using Genetic Algorithms**

## 3.6 Operative prospect

As shown in the previous chapter, the directional information content exploited in CR model inversion improves LAI estimation for two from three of the analyzed crops. Thus, LAI estimation from multiangular data by means of model inversion seems to perform reliable. Furthermore, it essentially does not require any ground information to be calibrated as for empirical approaches. On the other hand, there are limitations due to the directional sampling required for the determination of the ill-posed problem, for the model inversion parameterization and for optimizing computational time. Moreover, although CHRIS/PROBA mission has been operating much longer than foreseen, prospecting economical feasibility, nowadays, E.O. data at spatial scale and directional sampling as provided by this unique sensor are not available for on-request acquisition and commercial distribution.

Therefore, for this study the use of a simple vegetation index as an alternative approach to model inversion is also considered, giving an operative prospective for LAI estimation from E.O. data.

In this section the CLAIR model approach is applied and a comparison with CR model inversion is presented.

## 3.7 Effect of view angle on WDVI and CLAIR model

Near nadir satellite acquisitions are often requested to minimize the effect of solar angle and view position on directional reflectance due to non-Lambertian properties of natural surfaces (Osborne et al., 2002; Otterman et al., 1995; Serrano et al.,2000).

The effect and the persistence of reflectance anisotropy on vegetation indices based on band ratios were demonstrated by some authors using model simulation and ground radiometric measurements (see e.g. Woolley, 1971; Pinter et al., 1987; Rahman et al., 1999; Giardino, 2001).

For our case study this effect was evaluated considering the geometry observation first in the Principal Plane (PP) and then in the Orthogonal Plane (OP). The PP occurs when the azimuth angle between sensor and sun is equal to 0° and 180°. The OP is the plane orthogonal plane to the PP one.

The WDVI was computed by using model simulated reflectance for these two configurations as a function of view zenith angles ranging from 0° (nadir position) to 60°.

A relative variation of 16% on the WDVI was found in the PP (considering the hot-spot position - when phi = 0° - and the dark-spot position - when phi = 180° -, where phi is the difference between Sun and View azimuth Angles, SAA and VAA, respectively). A relative variation of 4% was observed in the OP (phi = 90°).

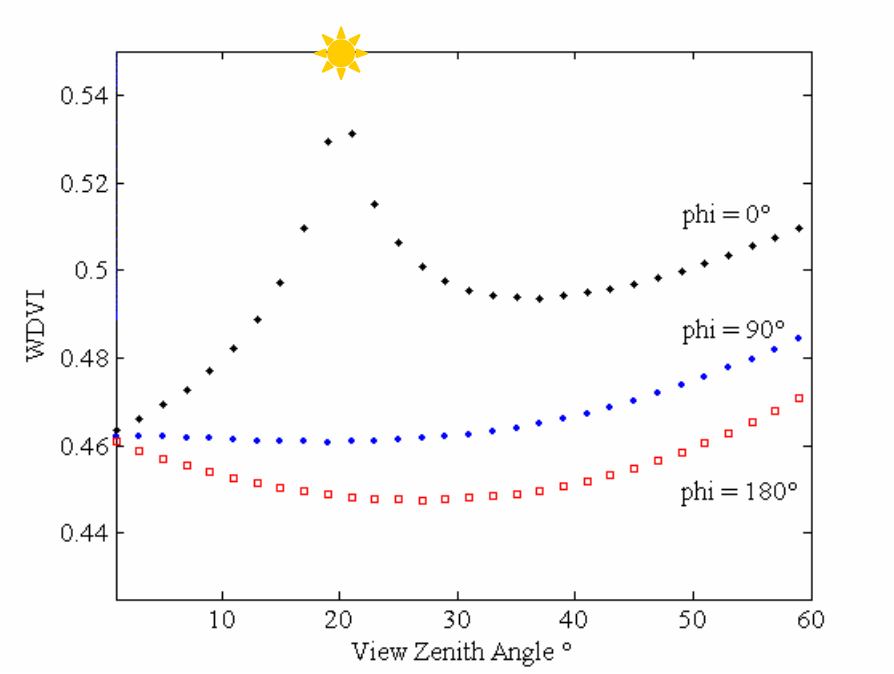


**Figure 24 Anisotropy of WDVI calculated from PSH model simulations, as a function of viewing zenith angle and three azimuth angle configurations (phi=0°, phi=90°, phi=180°, where phi is the difference between Sun and View azimuth Angles) (Sun zenith is 20°).**

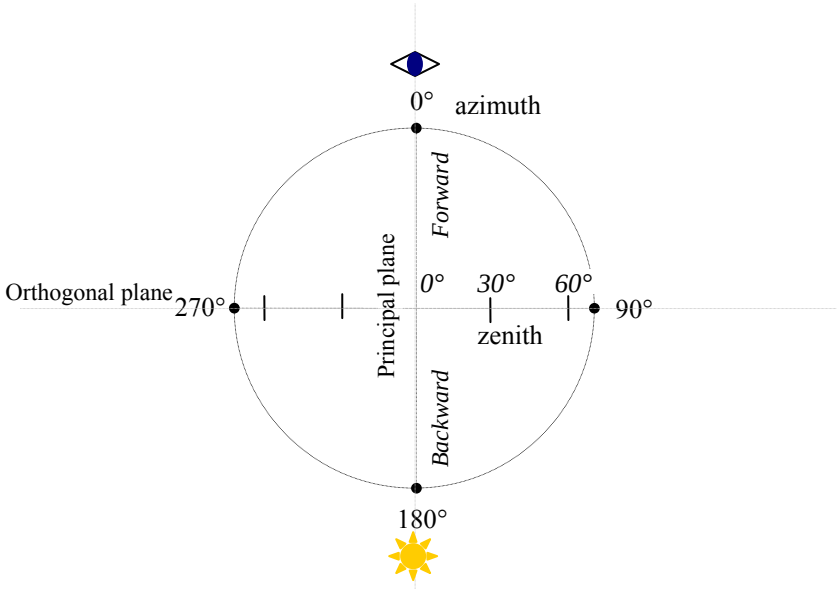


**Figure 25 Schematic representation of the acquisitions and observation geometry with azimuth and zenith coordinates in degrees. Definition of the principal and orthogonal planes.**

Considering CHRIS/PROBA geometric configuration, the difference on the WDVI for the closest to nadir acquisition ("A3", VZA=27.6°, phi= 137.2°) in respect to the WDVI calculated from nadir observation is about 2%. An error function was then computed for the CLAIR model, taking into account a variation of 20% on WDVI.

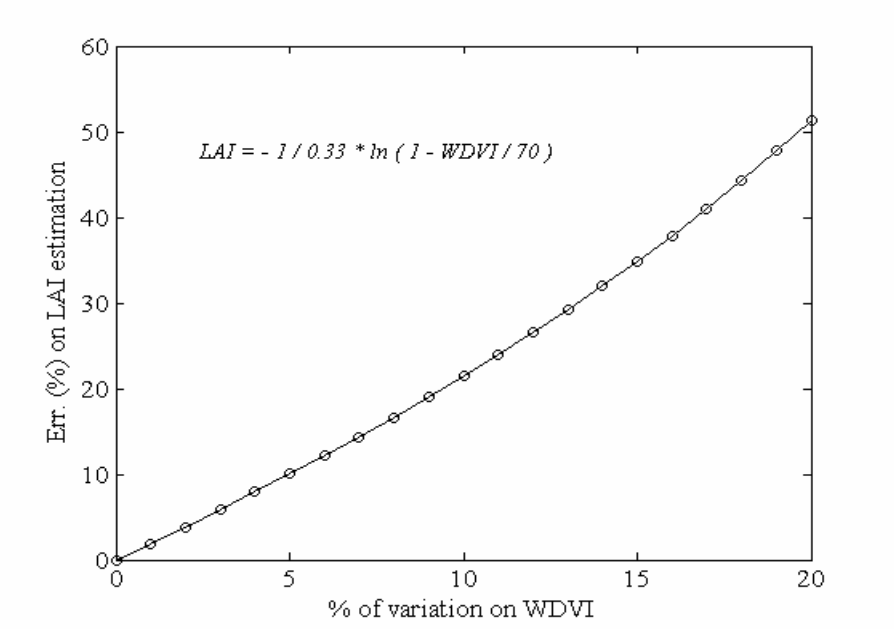


**Figure 26 Sensitivity of CLAIR model to error on LAI estimation due to percentage variations on WDVI**

## 3.8 CLAIR model results

The calibration and validation of the CLAIR model was carried out using two independent data sets of LAI measurements collected during the campaign. The broad red and infrared bands of the view angle closest to nadir ("A3") were considered (while broad red was integrated from band 21 to 28 and the infrared from band 39 to 54). The value of soil-line slope coefficient was calculated resulting in a value of 1.07 ($\rho_{si}/\rho_{sr}$), with $\alpha^* = 0.4$ and $WDVI_\infty = 6800$.

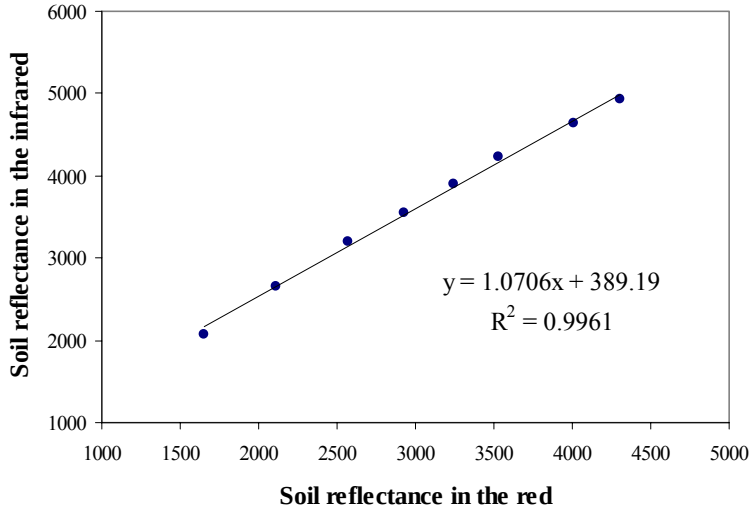


**Figure 27 Soil-line characteristics for Barrax site - 2003**

| *LAI estimation accuracy CLAIR model* | | |
|---|---|---|
| **CROP** | **$RMSE_{LAI}$** | **$RPE_{LAI}$** |
| *Alfalfa* | 0.68 | 35.3% |
| *Corn* | 0.45 | 9.0% |
| *Potato* | 0.67 | 12.1% |

**Table 18 LAI estimation accuracy by using CLAIR model. For each of the experiments, the LAI accuracy is evaluated in terms of root mean square error ($RMSE_{LAI}$) and relative percentage error ($RPE_{LAI}$).**

Comparing the two approaches for alfalfa, using similar spectral and directional information, the $RMSE_{LAI}$ values are close to each other: 0.68 (CLAIR, 1 angle, 2 bands) and 0.71 (PSH, 1 angle, 4 bands). With the best angular and spectral sampling (5 and 62 respectively), the physical approach improves the accuracy slightly less than 25%. As for corn, with similar information contents, the CLAIR model performs better than the PSH inversion: 0.45 (CLAIR, 1 angle, 2 bands) and 1.42 (PSH, 1 angle, 4 bands). Only by using 5 angles and 62 bands, model inversion provides comparable results to the empirical approach. For potato, in all cases the vegetation index approach performs better than the inversion of the PSH model.

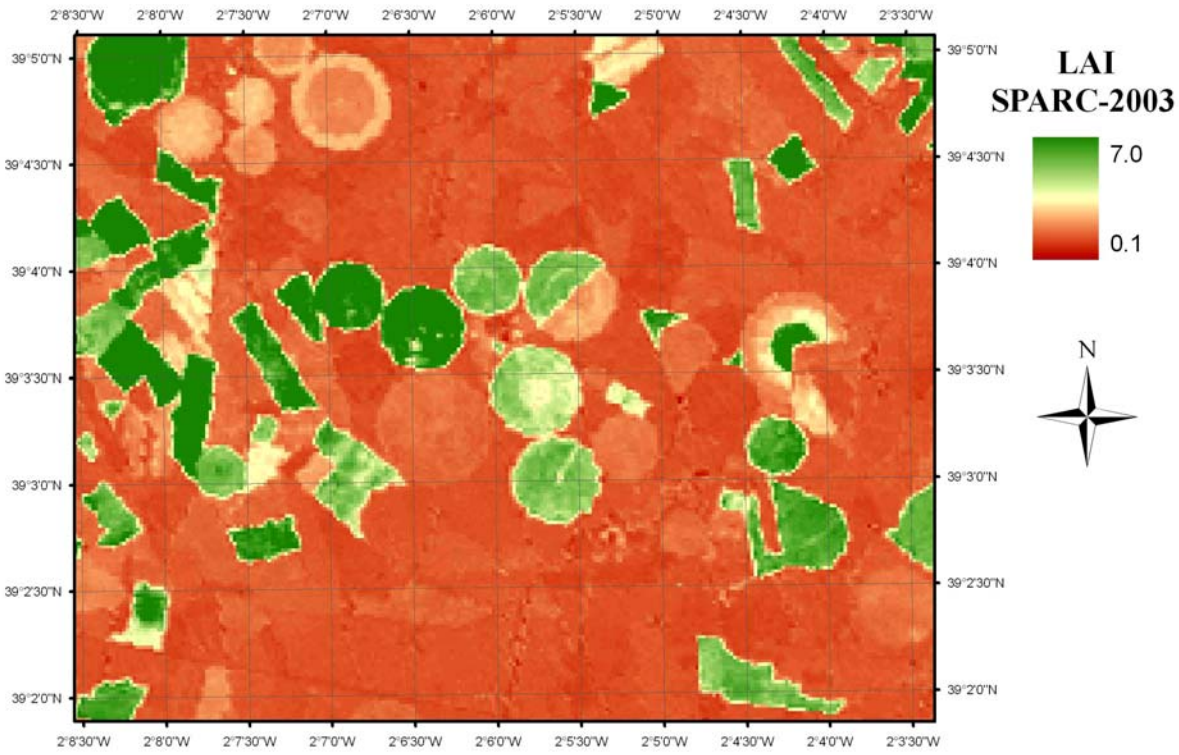


**Figure 28 LAI map obtained from LandsatTM-5 data by means of the CLAIR model - 15/July/2003**

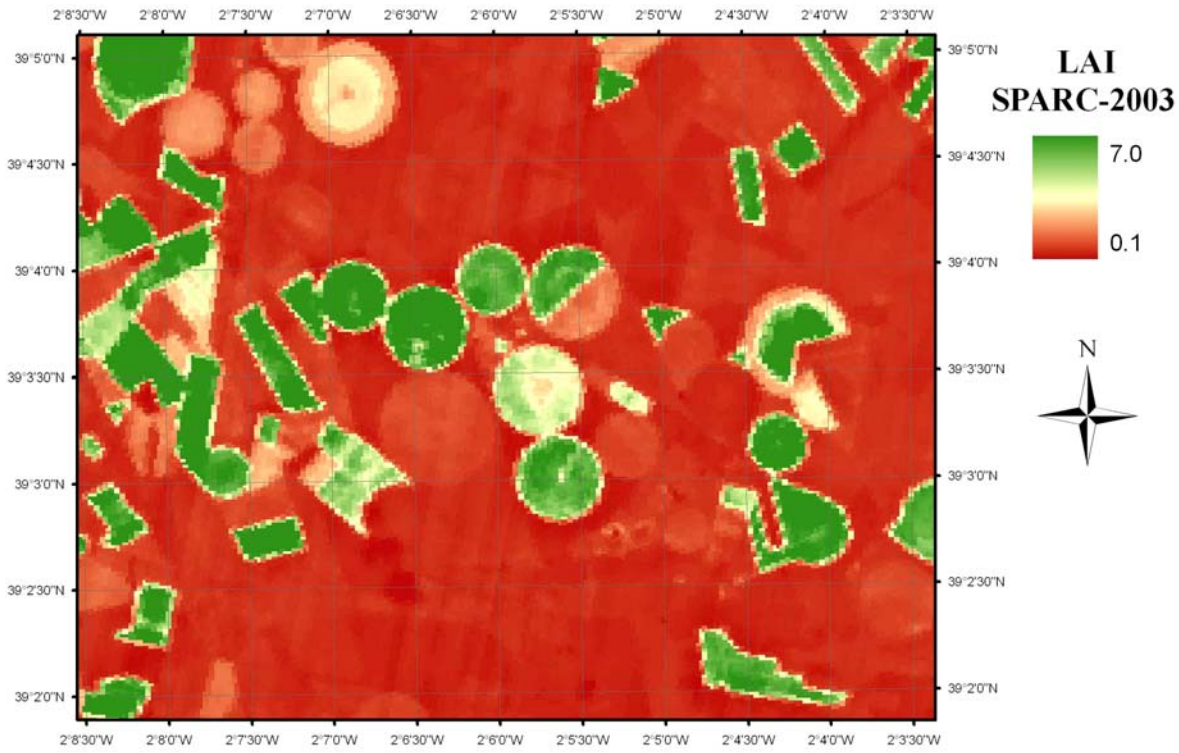


**Figure 29 LAI map obtained from CHRIS/PROBA "A3" data by means of the CLAIR model – 14/July/2003**

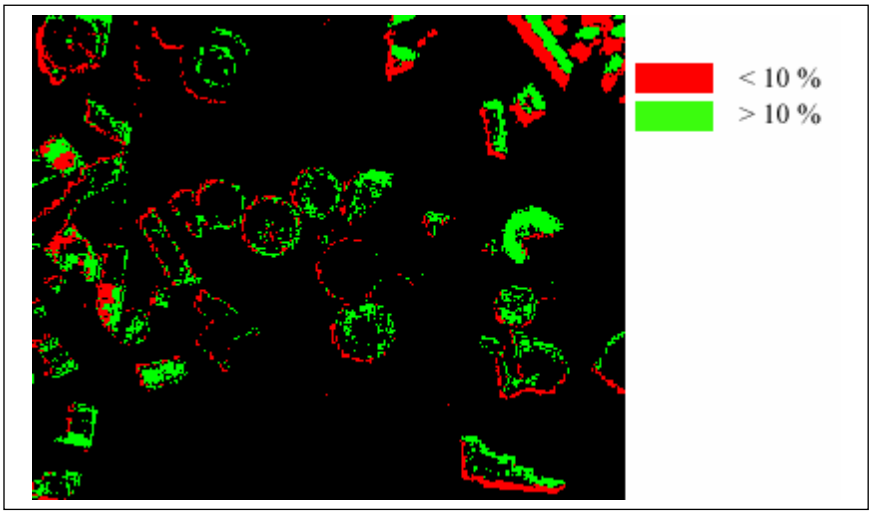


**Figure 30 The image shows the differences between LAI map obtained from LANDSAT and from CHRIS/PROBA. Areas that present a difference greater than 10% are displayed in green, whereas areas colored in red describe the areas with a difference less than 10%. The black the zones present equal distribution of LAI estimation.**

# *Chapter 4*

## 4 Conclusions

This work aimed to demonstrate processing and modelling techniques to assess the strengths and limitations of vegetation parameters retrieval from Earth Observation data, in particular from innovative experimental satellites.

In this context, the CHRIS/PROBA technology demonstration mission and the ESA SPARC campaign offered the scientific community the unique opportunity to exploit high spatial and spectral multiangular imagery from space.

The main objective of this study was to assess the importance of directional information sampled from space on the LAI estimation accuracy. The high dimensionality of this kind of data, with a complete exploitation of the spectral and directional domains of the canopy radiometric measurements, allowed us to validate the inversion of complex physical based models.

The effectiveness of the combined use of PROSPECT and SAILH models (PSH model) to simulate canopy BRDF with an acceptable accuracy could be demonstrated. In particular the importance of the soil reflectance component on the overall spectral reflectance could be shown. Thus, the use of a soil reflectance map of the area under investigation as well as the removal of the Lambertian surface hypothesis for the soil reflectance could lead to a more accurate BRDF modelling for sparse canopies. However, the goodness of the results obtained, at least for the crops under investigation, encouraged the use of these models in the inverse mode in order to retrieve vegetation parameters.

By using different optimization algorithms, the invertibility of the PSH model was proven by using noise-free synthetic-generated data. LAI estimates were reasonably accurate ($RPE_{LAI}$=10%). ALA was more accurately estimated with a mean percentage error of 2.2%. Effects of random Gaussian noise in synthetic data were also tested and parameters estimation remained accurate.

Results from model inversion by using satellite data showed that the directional information content improves LAI estimation for two of three of analyzed crops. In the best case (corn) a LAI RMSE of 0.41 was achieved by using 5 angles and 62 spectral bands with an improvement of almost 65% respect to 1 angle and 16 bands.

It seems also that the directional is predominant on the spectral information, suggesting the design of space-borne instruments in the future with better capabilities to sample the surface reflectance anisotropy.

A comparison analysis between the inversions of the physical-based model vs. an empirical approach was carried out. From an operational point of view, results obtained by inverting PSH model and exploiting the full CHRIS data are better or comparable to the ones from the empirical approach. On the one hand, the inversion process results highly demanding in terms of computational time and parameterization complexity, on the other hand it does not require any field measurements to be calibrated as the empirical approaches.

Conclusively, this work gives an operative perspective of current possibilities from single-view satellite data and how technical progress contributes to improve accuracies of parameter estimation, in particular for LAI retrieval.

## REFERENCES


Andrieu, B., Baret, F., Jacquemoud, S., Malthus T., Steven, M. (1997). Evaluation of an improved version of SAIL model to simulate bi-directional reflectance of sugar beet canopies. Remote Sensing of Environment, 60:247-257.

Atzberger, C., (2002). Object-based retrieval of structural and biochemical canopy characteristics using SAIL+PROSPECT canopy reflectance model: A numerical experiment. In J. Sobrino (Ed.), Recent advances in quantitative remote sensing, 129–138.

Atzberger, C., (2004). Object-based retrieval of biophysical canopy variables using neural nets and radiative transfer models. Remote Sensing of Environment, 93, 53–67.

Bacour, C., Jacquemoud, S., Leroy, M., Hautecoeur, O., Weiss, M., Prévot, L., Brugueir, N. and Chauki, H. (2002) Reliability of the estimation of vegetation characteristics by inversion of three canopy reflectance models on airborne POLDER data. Agronomie, 22, 555-565.

Baret, F., Guyot, G. (1991) Potentials and limits of vegetation indices for LAI and APAR assessment. Remote Sensing of Environment, 35, 161–173.

Baret, F., Jacquemoud, S., Hanocq, J.F. (1993) About the soil line concept in remote sensing. Advanced in space research, 13, 5 281-284.

Barnsley M.J., J. J. Settle, M. Cutter, D. Lobb, and F. Teston (2004). "The PROBA/CHRIS mission: A low-cost smallsat for hyperspectral, multiangle, observations of the earth surface and atmosphere," IEEE Trans. Geosci. Remote Sens., vol. 42, no. 7, pp. 1512–1520, Jul. 2004.

Broge, N.H., Leblanc, E. (2000). Comparing prediction power and stability of broadband and hyperspectral vegetation indices for estimation of green leaf area index and canopy chlorophyll density. Remote Sensing of Environment, 76, 156–172.

Chapman J W, Gower S T. (1991). Above-ground production and canopy dynamics in sugarmaple and red oak trees in southwestern Wisconsin. Can. J. For. Res. 21:1533–1543.

Chen J M, Black T. A. (1992). Defining leaf area index for non-flat leaves. Plant Cell Environ. 15:421–429.

Chen, J. (1996). Evaluation of vegetation indices and modified simple ratio for boreal applications. Can. J. Remote Sens., 22, 229–242

Clevers, J. (1989). The application of a weighted infrared-red vegetation index for estimating leaf area index by correcting for soil moisture. Remote Sensing of Environment, 29, 25-37.

Cutter M. and L. Johns (2004) "CHRIS data format report," Sira Technol. Ltd., Kent, U.K., Tech. Rep.

FAO (1998). Crop evapotraspiration. Guidelines for computing crop water requirements. Irrigation and Drainage Paper, 56.

Giardino C., (2001). Anisotropy of the reflected radiation field over natural surfaces. Ph.D. thesis.

Gates D M, Keegan H J, Schleter J C, Weidner V. P. (1965). Spectral properties of plants. Appl. Optics, 4:11–20.

Gausman H.W. (1974) Leaf reflectance of near-infrared. Photogramm. Eng. Remote Sens. 40:183–191.

Goel, N. S. (1988). Models of vegetation canopy reflectance, their use in estimation of biophysical parameters from reflectance data. Remote Sensing Reviews, 4, 1 – 212

Guanter, L., Alonso, L. , and Moreno, J., (2005) A Method for the Surface Reflectance Retrieval From PROBA/CHRIS Data Over Land: Application to ESA SPARC Campaigns, IEEE Transactions on Geoscience and Remote Sensing, 43(12), 2908-2917.

Huete, A R, (1987) Soil and sun angle interactions on partial canopy spectra. Int. J. Remote Sens. 8, 1307–1317.

Hunt, E., R. Piper, S. C., Nemani, R., Keeling, C. D., Otto, R. D., Running, S. W. (1996). Global net carbon exchange and intra-annual atmospheric CO2 concentrations predicted by an ecosystem simulation model and three-dimensional atmospheric transport model. Global Biogeochemical Cycles, 10:431-456.

Jacquemoud, S. & Baret, F. (1990). PROSPECT: A model of leaf optical properties spectra, Remote Sensing of Environment, 34, pp. 75-91.
Jensen, M.E., M.E., Burman M.E., Allen R.G. (1990). Evapotraspiration and irrigation water requirements. ASCE Manual.

Jochum, O.M.A., Calera, A. et al., (2006) Operational space-assisted irrigation advisory service: overview of and lesson learned from the project Demeter. AIP, American Institute of Physics ISBN: 0-7354-0346-5

Kimes, D. S., Knyazikhin, Y., Privette, J. L., Abuelgasim, A. A., & Gao,F. (2000). Inversion methods for physically-based models. Remote Sensing of Environment, 18, 381– 439.

Knipling E.B. (1970) Physical and physiological basis for the reflectance of visible and near-infrared radiation from vegetation. Remote Sens. Environ. 1:155–159.

Laine Boresjö Bronge, SwedPower AB. (2004). Satellite remote sensing for estimating leaf area index, FPAR and primary production, SKB, ISSN 1402-3091, March 2004.

Li, X. and Strahler, A.H., (1995): A Hybrid Geometric Optical-Radiative Transfer Approach for Modeling Albedo and Directional Reflectance of Discontinuous Canopies. IEEE TRANS.ACTJONS ON GEOSCIENCE AND REMOTE SFNSJNG. VOL. 33, NO. 2. MARCH 1995

Major D., Schaalje G., Wiegand C., Blad B. (1992), Accuracy and sensitivity analysis of SAIL model-predicted reflectance of maize. Remote Sensing of Environment, 41:61-70.

Myneni, R. B., Ross, J., & Asrar, G. (1989). A review on the theory of photon transport in leaf canopies. Agricultural and Forest Meteorology, 45, 1 – 153.

Nicodemus, F. E., J. C. Richmond, J. J. Hsia, I. W. Ginsberg, and T. Limperis. (1977). Geometrical Considerations and Nomenclature for Reflectance, NBS Monogr., No. 160, National Bureau of Standards, U.S. Department of Commerce, 52 pp.

Pinter P.J., Zipoli G., Maracchi G. and Reginato R.J. (1987). Influence of topography and sensor view angles on NIR/red ratio and greeneess vegetation indices of wheat. Int. J. Remote Sens. 8:953-957.

Pinty, B., Gobron, N., Widlowski, J.-L., Gerstl, S. A. W., Verstraete, M.M., Antunes, M., Bacour, C., Gascon, F., Gastellu, J.-P., Goel, N., Jacquemoud, S., North, P., Qin, W. and Thompson, R., (2000). The RAdiation transfer Model Intercomparison (RAMI) Exercise, Journal of Geophysical Research - IWMMM-2.

Qiang, L., Qinhuo, L., Menenti, M., (2003), Spatial resolution limits in extraction of BRDF feature from remote sensing image data, IEEE Trans. Geosci. Remote Sens. 0-7803-7930-6

Sellers P J, (1985). Canopy reflectance, photosynthesis and transpiration. Int. J. Remote Sens. 6:1335–1372.

Sellers P.J. (1987). Canopy reflectance, photosynthesis and transpiration, II. The role of biophysics in the linearity of their interdependence. Remote Sens. Environ. 21:143–183.

Sellers P. J. (1989). Vegetation-canopy spectral reflectance and biophysical properties. In G. Asrar (Ed), Theory and Applications of Optical remote Sensing, New York:Wiley.

Sellers, P.J., Los, S. O., Tucker, C.J., Justice, C.O., Dazlich, D.A., Collatz, G.J., Randall, D.A. (1996). A revised land surface parameterisation (SiB2) for atmospheric GCMs: Part II. The generation of global fields of terrestrial biophysical parameters from satellite data. Journal of Climate, 9:706-737.

Tucker C. J. (1978). A comparison of satellite sensor bands for monitoring vegetation. Photogramm. Eng. Remote Sens. 44:1369–1380.

Tucker C J, Sellers P.J. (1986). Satellite remote sensing of primary production. Int. J. Remote Sens. 7:1395–1416.

Verhoef , W. (1984). Light scattering by leaf layers with application to canopy reflectance modelling: The SAIL model, Remote Sensing of Environment, 16, 125-141.

Verhoef, W. (1998). Theory of radiative transfer models applied in optical remote sensing of vegetation canopies. Ph.D. thesis. National Aerospace Lab., Amsterdam, The Netherlands

Verstraete, M., Pinty, B., & Myneni, R. B. (1996). Potential and limitations of information extraction on the terrestrial biosphere from satellite remote sensing. Remote Sensing of Environment, 58, 201– 214.

Vuolo, F., De Michele, C. and Lazzaro, U., (2006). Succes Stories: analysis and evaluation of Italian case-study of DEMETER in the Destra Sele plain, AIP, American Institute of Physics ISBN: 0-7354-0346-5

Walter-Shea A., Privette J., Cornell D., Mesarch M.A., Hays C.J (1997), Relation between directional spectral vegetation indices and leaf are and absorbed radiation in Alfalfa, Remote Sensing of Environment, 61, 162-177.

Woolley J.T. (1971) Reflectance and transmittance of light by leaves. Plant Phys. 47:656–662